Bioactive Materials 36 (2024) 203–220

Contents lists available at ScienceDirect

Bioactive Materials

journal homepage: www.keaipublishing.com/en/journals/bioactive-materials

Robust reactive oxygen species modulator hitchhiking yeast microcapsules for colitis alleviation by trilogically intestinal microenvironment renovation

Jintao Li [a,1], Jian Song [b,1], Zhichao Deng [c], Jian Yang [a], Xiaoqin Wang [d], Bowen Gao [c], Yuanyuan Zhu [c], Mei Yang [e], Dingpei Long [f], Xiaoqin Luo [a], Mingxin Zhang [g,**], Mingzhen Zhang [c,*], Runqing Li [a,***]

[a] Department of Radiology, the First Affiliated Hospital, School of Public Health, Xi'an Jiaotong University, Xi'an, Shaanxi, 710061, China
[b] Institute of Cardiovascular Sciences, Guangxi Academy of Medical Sciences, the People's Hospital of Guangxi Zhuang Autonomous Region, Nanning, Guangxi, 530021, China
[c] School of Basic Medical Sciences, Xi'an Jiaotong University, Xi'an, Shaanxi, 710061, China
[d] Department of Clinical Laboratory, the First Affiliated Hospital of Xi'an Jiaotong University, Xi'an, Shaanxi, 710061, China
[e] Department of Thoracic Surgery, the First Affiliated Hospital of Xi'an Jiaotong University, Xi'an, Shaanxi, 710061, China
[f] State Key Laboratory of Resource Insects, Institute of Sericulture and Systems Biology, Southwest University, Chongqing, 400715, China
[g] Department of Gastroenterology, The First Affiliated Hospital of Xi'an Medical University, Xi'an, Shaanxi, 710077, China

ARTICLE INFO

Keywords:
Ulcerative colitis
Metal polyphenol network
Reactive oxygen species
Yeast microcapsules
Intestinal microenvironment

ABSTRACT

Ulcerative colitis (UC) is characterized by chronic inflammatory processes of the intestinal tract of unknown origin. Current treatments lack understanding on how to effectively alleviate oxidative stress, relieve inflammation, as well as modulate gut microbiota for maintaining intestinal homeostasis synchronously. In this study, a novel drug delivery system based on a metal polyphenol network (MPN) was constructed via metal coordination between epigallocatechin gallate (EGCG) and Fe^{3+}. Curcumin (Cur), an active polyphenolic compound, with distinguished anti-inflammatory activity was assembled and encapsulated into MPN to generate Cur-MPN. The obtained Cur-MPN could serve as a robust reactive oxygen species modulator by efficiently scavenging superoxide radical ($O_2^{\bullet-}$) as well as hydroxyl radical (·OH). By hitchhiking yeast microcapsule (YM), Cur-MPN was then encapsulated into YM to obtain CM@YM. Our findings demonstrated that CM@YM was able to protect Cur-MPN to withstand the harsh gastrointestinal environment and enhance the targeting and retention abilities of the inflamed colon. When administered orally, CM@YM could alleviate DSS-induced colitis with protective and therapeutic effects by scavenging ROS, reducing pro-inflammatory cytokines, and regulating the polarization of macrophages to M1, thus restoring barrier function and maintaining intestinal homeostasis. Importantly, CM@YM also modulated the gut microbiome to a favorable state by improving bacterial diversity and transforming the compositional structure to an anti-inflammatory phenotype as well as increasing the content of short-chain fatty acids (SCFA) (such as acetic acid, propionic acid, and butyric acid). Collectively, with excellent biocompatibility, our findings indicate that synergistically regulating intestinal microenvironment will be a promising approach for UC.

Peer review under responsibility of KeAi Communications Co., Ltd.
* Authors for Correspondence
** Authors for Correspondence
*** Authors for correspondence
E-mail addresses: zmx3115@xiyi.edu.cn (M. Zhang), mzhang21@xjtu.edu.cn (M. Zhang), lirunqing718@xjtu.edu.cn (R. Li).
[1] These authors contribute equally to this work.

https://doi.org/10.1016/j.bioactmat.2024.02.033
Received 10 December 2023; Received in revised form 21 February 2024; Accepted 25 February 2024

1. Introduction

Ulcerative colitis (UC), also known as inflammatory bowel disease (IBD), is an idiopathic inflammatory disease affecting the ileum, rectum, and colon. The global prevalence of IBD is increasing each year, with common complications [1,2]. Clinical manifestations typically include diarrhea, abdominal pain, vomiting, tenesmus, and bloody stools. In severe cases, colorectal resection may be necessary, significantly impacting patients' quality of life [3]. IBD is characterized by complex pathology, including excessive apoptosis of intestinal epithelial cells (IEC), abnormal intestinal flora, disruption of the intestinal barrier, and elevated levels of inflammation and reactive oxygen species (ROS) [4–8]. Acute inflammation triggers the differentiation of infiltrating monocytes into activated macrophages in the lamina propria, intensifying the inflammatory response by continuously secreting high levels of inflammatory cytokines, chemokines, and ROS. This exacerbates IEC apoptosis, dysfunctional intestinal barrier, and ecological dysregulation of the intestinal microbiome [9–11].

The current clinical drugs used to treat IBD face two major challenges: lack of IBD targeting, resulting in systemic adverse reactions and life-threatening side effects, and providing only temporary relief with anti-inflammatory medication while failing to address the underlying imbalance of the intestinal flora, leading to recurrent disease [12,13]. Mild to moderate colitis is typically treated with oral 5-ASA drugs as first-line therapy, while glucocorticoid therapy is employed for acutely active disease or when 5-ASA fails to induce remission [13]. Moderate-to-severe colitis patients are treated with immunosuppressants, biologics, or a combination of both [14]. However, these treatments often have significant toxic side effects and do not rectify the dysregulated gut microflora [15,16]. For example, glucocorticoids tend to induce or exacerbate infections, and mercaptopurines increase the risk of nonmelanoma skin cancers [17,18]. Therefore, the development of innovative therapies that target colitis, remodel the immune homeostasis of the intestinal mucosa by regulating the intestinal flora, and efficiently scavenge ROS is crucial for effective IBD treatment.

Oral medications are preferred for IBD treatment due to their convenience, cost-effectiveness, and high patient compliance. However, they face challenges such as gastric acid degradation, rapid metabolism, elimination rates, and lack of drug targeting [19]. Yeast microcapsules (YM), a natural carrier for oral microencapsulation, can protect drugs from gastric acid degradation [20,21]. YM mainly consists of β-glucan, which can be recognized by macrophages through various pattern recognition receptors, including complement receptor 3 and dectin-1 receptor [22–24]. Moreover, the mannan in YM serves as a prebiotic for beneficial bacteria in the intestinal tract, promoting beneficial bacteria proliferation, inhibiting harmful bacteria growth, and regulating the intestinal flora of IBD patients [25–27]. Curcumin (Cur), a polyphenol extracted from turmeric rhizomes used as a food coloring agent, exhibits antimicrobial, antioxidant, anti-apoptotic, anti-tumor, and anti-metastatic activities, making it a promising biomedical agent [28–31]. However, Cur suffers from poor solubility in water, photodegradation, chemical instability, and low bioavailability, limiting its direct use for colitis treatment [32,33]. Epigallocatechin Gallate (EGCG), a type of tea polyphenol and FDA-approved natural food ingredient, forms a metal polyphenol network (MPN) through coordination with metal ions (e.g., Fe, Cu, and Zn) [34–36]. Based on this, the present study constructed an MPN by coordinating EGCG with Fe^{3+} and loading Cur into it to synthesize Cur-MPN. Cur-MPN not only significantly improves the bioavailability of Cur but also demonstrates stronger anti-inflammatory and antioxidant activities when combined with EGCG and Cur [37]. Subsequently, Cur-MPN was loaded into YM, resulting in CM@YM, which exhibited excellent biocompatibility and targeted delivery of the ROS scavenger Cur-MPN to the site of inflammation. This approach enables the regulation of IBD through anti-inflammation and the remodeling of the intestinal microecology.

In this work, we designed a colon-targeted oral drug delivery system with a high safety profile for IBD treatment. Cur was encapsulated in an MPN formed by EGCG and Fe^{3+} to produce anti-inflammatory nanoparticles with high biocompatibility. These nanoparticles were further encapsulated in YM, allowing for protection from gastric degradation and targeted delivery to the site of intestinal inflammation through specific binding to the dectin-1 receptor on macrophages (Scheme 1). This natural product-targeted oral delivery system provides a new approach to the treatment of IBD through anti-inflammation, antioxidation, and modulation of the intestinal flora.

2. Materials and methods

2.1. Materials

Active baker's Yeast was purchased from Angel Yeast Co., Ltd. (Yichang, China). Curcumin and EGCG were purchased from Macklin (Shanghai, China). DSS was purchased from Yeasen (Shanghai, China). Phosphate buffer saline (PBS) was purchased from Sevier (Wuhan, China). 2,7-dichlorofluorescein diacetate (DCFH-DA) was purchased from Beyotime Biotechnology Co., Ltd. Fluorescent lipophilic dyes (DiL and DiR) were purchased from Promokine (Heidelberg, Germany). MTT, myeloperoxidase (MPO) assay kit, lipopolysaccharides (LPS), and antibodies (CD86, CD80, and CD206) were purchased from Meilun Bio (Dalian, China).

2.2. Preparation of Cur-MPN

To prepare Cur-MPN, Cur was first dissolved in dimethyl sulfoxide (DMSO) to obtain a stock solution. Then, 50 μL of the Cur stock solution was added to 5 mL of tris buffer (10 mM, pH 7.4) and vigorously stirred for 5 min. Subsequently, 50 μL of EGCG solution and 50 μL of $FeCl_3$ solution were added sequentially to the above dispersion under stirring. The ratio of Cur: EGCG: Fe^{3+} was 1:1:2. The mixture was then centrifuged at 10,000 rpm for 5 min, and the resulting precipitate was collected. The collected precipitate was washed with water multiple times to remove any unbound components. The resulting precipitate is referred to as Cur-MPN.

2.3. Preparation of CM@YM

Firstly, 20 g of yeast cells were suspended in 300 mL of 1 M sodium hydroxide and the suspension was heated at 80 °C for 1 h. Subsequently dispersed in an aqueous solution of pH 4 and incubated at 60 °C for 1 h. After cooling to room temperature the lysates of yeast cells were centrifuged at 3000 rpm for 10 min to obtain insoluble material containing cell walls. The resulting sample was rinsed four times with 100 mL of isopropanol, rinsed again with acetone, and collected by centrifugation to obtain the yeast cell wall, which was vacuum-dried at room temperature. Subsequently, 5 mg of YM was vortex-immersed into 1 mL of Cur-MPN dispersion for 5 min. After further stirring at 37 °C for 2 h, the sample was centrifuged at 10,000 rpm for 5 min, and the precipitate was then dispersed in ultrapure water. The unencapsulated Cur-MPN was removed by centrifugation at 3000 rpm for 5 min. After which the collected CM@YM was resuspended in ultrapure water and lyophilized under vacuum to obtain CM@YM powder.

2.4. Characterization of Cur-MPN and CM@YM

A dynamic light scattering (Anton Paar, Litesizer TM 500) was applied to monitor the hydrodynamic diameter (Dh) and polydispersity index (PDI) of Cur-MPN and CM@YM. The zeta potential of the Cur-MPN and CM@YM was measured by Malvern Zetasizer Nano ZS90 at room temperature. The UV–vis absorption spectra and the FTIR spectra of Cur-MPN were recorded by an ultraviolet spectrophotometer (Thermo-Scientific, Evolution 201) and Fourier transformation infrared spectrophotometer (Bruker, Germany). X-ray photoelectron

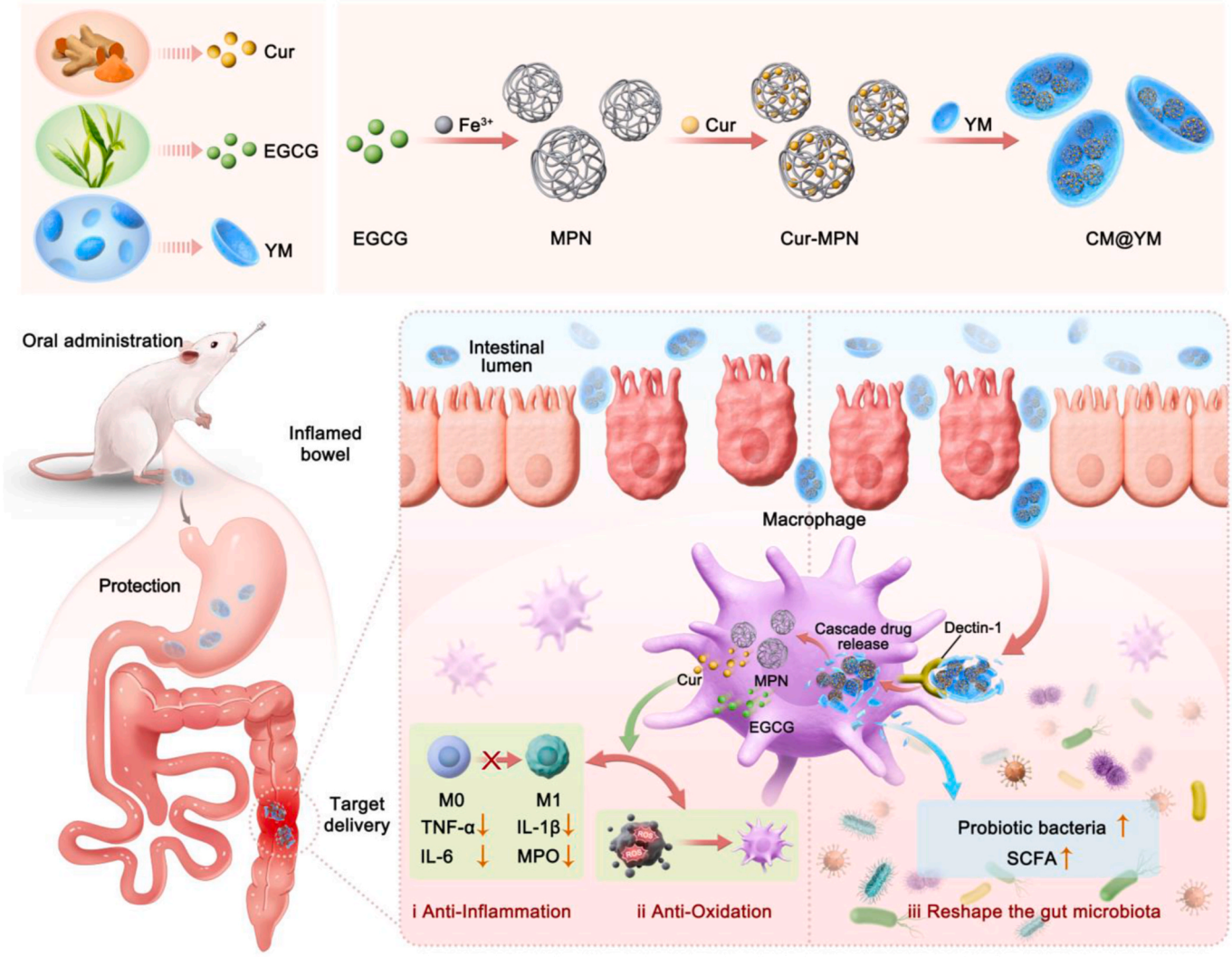

Scheme 1. Schematic illustration of CM@YM preparation and potential therapeutic mechanisms. Curcumin was self-assembled into the MPN formed by the coordination of EGCG and Fe^{3+} to form the ROS scavenger Cur-MPN, which was then encapsulated in YM by chemical precipitation to obtain CM@YM. By oral administration, CM@YM was able to efficiently deliver the drug to the colon site and retain there for a prolonged time through the hostile gastrointestinal environment, and was specifically recognized by macrophages in the intestine. In addition, CM@YM could reduce the production of pro-inflammatory cytokines, inhibit type 1 macrophage differentiation, and promote epithelial barrier repair. Importantly, CM@YM also restored the abundance and diversity of gut microbiota, significantly increasing the abundance of probiotics, suppressing the abundance of harmful flora, and increasing the content of SCFA.

spectroscopy (XPS, Thermo Fisher ESCALAB Xi+) was used to characterize the elemental content and valence states of Cur-MPN. The morphology of Cur-MPN and CM@YM was characterized by transmission electron microscopy (TEM, JEM-2100) at 200 keV accelerating voltage. The surface structures of YM and CM@YM were characterized by scanning electron microscopy (SEM, JSM-IT800, Japan) and energy dispersive X-ray spectroscopy (EDS, OXFORD AZtecLive Utim Max65, England). To further observe the encapsulation of Cur-MPN by YM, Cur-MPN containing Dil was prepared using Dil (red) as a fluorescent marker, and YM was selectively stained with calcium fluorescent white dye (blue) and CLSM was used for observation.

2.5. Drug encapsulation efficiency (EE) of Cur-MPN and CM@YM

To calculate the EE of Cur in Cur-MPN and CM@YM, the following approach was applied: a small amount of HCl was added to the Cur-MPN and CM@YM collected by centrifugation, followed by the addition of 75% ethanol-water solution, and Cur was extracted by ultrasonication for 30 min. Finally, the content of Cur was tested by recording the absorbance at 430 nm. The drug EE was calculated using the following equation: EE (%) = Actual Cur/Theory Cur × 100%

2.6. SEM determination of YM in different environments

The obtained YM was incubated in simulated gastric fluid (SGF) at 37 °C for 2 h, and the YM was collected by centrifugation, and then a portion of the incubated YM was placed in simulated intestinal fluid (SIF) supplemented with 0.5 % β-glucanase for 4 h, and the final YM was collected by centrifugation. All the YM samples were subjected to SEM for the surface structural characterization.

2.7. In vitro drug release profile

The curcumin and EGCG release profiles from different formulations were evaluated using the dialysis method. Briefly, 3 mL of Cur-MPN and CM@YM were added to dialysis bags (molecular weight cutoff, 1000 Da), respectively. The bags containing Cur-MPN and CM@YM were submerged in 30 mL of SGF or SIF to further release profile evaluation.

Meanwhile, another bag, which contains CM@YM was evaluated in a 30 mL SIF medium with 5% β-glucanase. Four groups of samples were shaken at 37 °C with a 100 rpm stir. At proper time points (0.5, 1, 2, 4, 6, 8, 10, 12, and 24 h), 1 mL of outer solution was collected for measurement, and then, 1 mL of fresh release medium was added, the cumulative release (%) was measured using UV–vis absorption spectra.

2.8. ROS scavenging ability and stability test

Cur-MPN was incubated in simulated intestinal fluid (SIF) or inflammatory simulated intestinal fluid (SICF) at 37 °C for 2 h. Cur-MPN was then separated by centrifugation, and the obtained Cur-MPN was used for the SOD enzyme activity assay, the ABTS+• free radical scavenging assay, and the TMB assay.

ESR assay: 100 mM DMPO, 25 μM DTPA, 0.5 mM HYP, 0.1 U/mL XOD, and various concentrations of Cur-MPN were mixed in PBS (pH = 7.4) to produce $O_2^{\bullet-}$ by the hypoxanthine/xanthine oxidase (HYP/XOD) system, and the ESR spectra of BMPO/·OOH were recorded after 2 min. The Fenton reaction was used to generate ·OH by mixing 100 mM DMPO, 1.0 mM $FeSO_4$, 1.0 mM H_2O_2, and various concentrations of Cur-MPN in ddH_2O and the ESR spectra of DMPO/·OH were recorded after 2 min.

SOD enzyme activity assay: The SOD enzyme activity of Cur-MPN was measured using a superoxide dismutase assay kit developed by Dojindo Research Institute of Chemistry (Dojindo) at concentrations of 10, 20, 50, 100, and 150 μg/mL.

ABTS+• radical assay: initially, ABTS+• radicals were prepared by mixing ABTS (7 mM) and potassium persulfate ($K_2S_2O_8$, 2.45 mM) at 4 °C overnight. Then, appropriate concentrations (0.5, 1, 2, 5, and 10 μg/mL) of Cur-MPN were incubated with ABTS+• for 10 min, and its absorption at 734 nm was recorded.

TMB assay: since the hydroxyl radical (·OH) produced by the Fenton reaction oxidizes TMB to oxTMB, the adsorption of oxTMB reflects the ability of Cur-MPN to remove ·OH. Fenton's reagent (Fe^{2+}: 10 μM; H_2O_2: 3 mM) was mixed and then incubated with Cur-MPN (2.5, 5, 10, 20, and 50 μg/mL). After 10 min of reaction, oxTMB was monitored by UV spectrophotometer.

TA Indirect Method: Hydrogen peroxide can produce a large amount of ·OH under UV irradiation, and ·OH will react with TA to form fluorescent 2-dihydroxyterephthalic acid (excitation wavelength 320 nm, emission wavelength 425 nm). A PBS solution (pH 7.4) containing 5 mM H_2O_2 and TA (0.5 mM) was irradiated with UV for 15 min, then Cur-MPN was added at different concentrations, and the fluorescence intensity of the mixture was recorded.

2.9. Cell culture

Human colon epithelial cells (FHC) and mouse mononuclear macrophages (RAW 264.7) were cultured in DMEM medium normally supplemented with 10% fetal bovine serum (FBS) and 1% penicillin/streptomycin at 37 °C and 5% CO_2, respectively.

2.10. Cell targeting

Preparation of DiL-loaded Cur-MPN and CM@YM for cellular uptake studies. RAW 264.7 cells and FHC cells were incubated in 35 mm confocal dishes at a density of 1×10^5 cells/well for 24 h, respectively, and then RAW 264.7 cells and FHC cells were co-cultured with Cur-MPN and CM@YM, respectively, for 4 h. In the inhibitor group, cells were pretreated with laminarin (1 mg/mL) for 3 h to achieve a specific inhibitory effect on dectin-1. Cells were then fixed using 4% paraformaldehyde and washed several times. The cells were stained with DAPI and washed again several times. Cell uptake images were obtained by CLSM.

2.11. Mitochondria/lysosome localization

After RAW 264.7 cells were co-incubated with NPs for 4 h, Mito-Tracker/Lyso-Tracker was added into the cell medium according to different proportions and continued to incubate at 37 °C for 45 min. The medium was removed and cells were washed twice with PBS before taking out the glass climbing plate and sealing it with DAPI.

2.12. Intracellular antioxidant and anti-inflammatory experiments

RAW 264.7 cells were seeded in 96-well plates and then co-incubated with Cur-MPN or CM@YM (20 μg/mL) and H_2O_2 (1 mM) for 10 h. The RAW 264.7 cells after co-incubation with Cur-MPN or CM@YM and H_2O_2 were stained with 2,7-dichlorofluorescein diacetate (DCFH-DA, 20 μM) and dihydroethidium (DHE, 1 μM) for 30 min to quantify the intracellular ROS levels. In addition, these above-treated RAW 264.7 cells were also stained with Calcein AM (AM, green, live cell) and propidium iodide (PI, red, dead cell) for 15 min to determine the cell protection by Cur-MPN or CM@YM. Finally, all the images were acquired by CLSM.

RAW 264.7 cells were inoculated in 96-well plates and then co-incubated with Cur-MPN or CM@YM (10, 20, 40 μg/mL) and H_2O_2 (1 mM) for 10 h. Standard MTT assays were performed to test relative cell viability.

RAW 264.7 cells after co-incubation with Cur-MPN and CM@YM (20 μg/mL) and LPS (40 μg/mL) were stained with 2,7-dichlorofluorescein diacetate (DCFH-DA, 20 μM) for 1 h to quantify intracellular ROS levels. Cell images were observed by CLSM and further quantified by flow cytometry.

2.13. Macrophage polarization assay

Inoculated with RAW 264.7, the cells were incubated with 20 μg/mL of YM, Cur-MPN, and CM@YM, respectively, for 24 h, and then incubated with 40 μg/mL lipopolysaccharide (LPS) overnight. The degree of macrophage polarization was assessed by staining the above RAW 264.7 with CD 80 markers, followed by flow cytometry assay.

2.14. Evaluation of intracellular biocompatibility

RAW 264.7 cells were incubated in 96-well plates at a density of 1×10^4 cells/well for 24 h. The wall-adherent cells were washed with PBS, and then the cells were co-incubated with 5, 10, 20, 50, 100, and 200 μg/mL of Cur-MPN and CM@YM for 24 h and 48 h. The control cells were cultured in DMEM, and the cell viability was determined by MTT assay. Absorbance was measured at 490 nm using a 96-well enzyme labeler. Data were expressed as mean ± SD.

2.15. Animals

Female C57BL/6 mice were purchased from Xi'an Keao Biotechnology Co., Ltd. Female Kunming mice were obtained from the Experimental Animal Center of Xi'an Jiaotong University. The animals were kept under 22–25 °C, 65 ± 5% humidity with a 12 h light-dark cycle, and fed regular and free drinking water. All experiments complied with the Institutional Animal Care and Use Committee at Xi'an Jiaotong University.

2.16. In vivo biocompatibility evaluation

Healthy mice were randomly divided into three groups: the control group, the Cur-MPN group, and the CM@YM group. The mice in the control group were gavaged with water, and the other two groups were gavaged with the corresponding drug (40 mg/kg/d). All mice were gavaged for three consecutive days, and the mice were euthanized seven days after the end of the gavage. Subsequently, major organs (heart,

liver, spleen, lungs, kidneys, and colon) and blood were harvested. H&E staining was performed to analyze the histological changes of the organs and whole blood samples were used for routine and blood biochemical assay analysis.

2.17. In vivo biodistribution

DiR-labeled nanosystems were firstly prepared (at a dose of 0.75 mg/kg DiR), and secondly, healthy C57 mice were randomly divided into three groups: the DiR group, the Cur-MPN group, and then healthy and colitis C57 mice were each divided into three groups: the Free DiR group, the Cur-MPN group, and the CM @YM group. Then the in vivo distribution of nanomaterials was detected by NIR in vivo small animal imager at 3 h, 6 h, 12 h, and 24 h after gavage administration. Mice were executed at the endpoint and the gastrointestinal tract tissue was removed for ex vivo fluorescence imaging.

2.18. In vivo therapeutic effect

The DSS-induced colitis mouse model was selected for in vivo experiments. To verify the efficacy of Cur-MPN@YM in treating colitis, firstly, female C57BL/6 mice were randomized and acclimatized for one week. Subsequently, the experiments were conducted according to the modeling protocol of treatment or delayed treatment as described above. Body weight changes and DAI indices of the mice were measured daily during the experiment and recorded according to a standard scoring system. After the mice were executed, the colon and cecum were separated, and the length of the colon was measured and photographed. The colon was then separated from the cecum and washed thoroughly with PBS several times until no feces or blood was present and drained on filter paper. A section of the colon sample was cut for subsequent histopathologic observation in H&E sections and immunofluorescence sections. Meanwhile, approximately 100 mg of colon segment was cut from each sample and the segment was accurately weighed. The sections

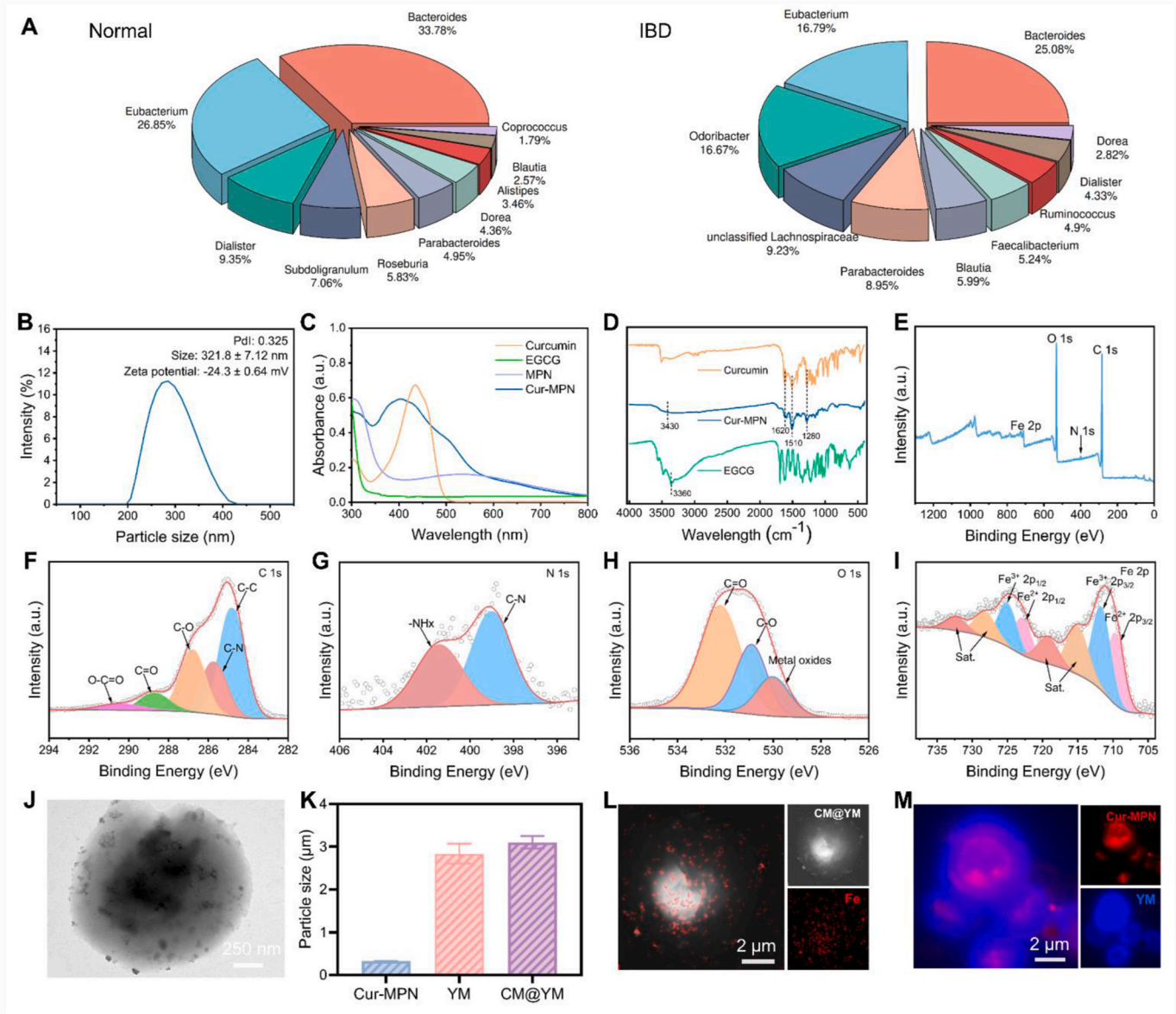

Fig. 1. Preparation and characterization of Cur-MPN and CM@YM. (A) Composition of the intestinal flora in normal and IBD patients at the genus level. (B) Representative hydrodynamic diameters of Cur-MPN. (C) UV–vis-spectra of EGCG, Curcumin, MPN and Cur-MPN. (D) FTIR spectra of EGCG, Curcumin and Cur-MPN. (E) Wide-range XPS patterns of Cur-MPN. C1 s (F), N1 s (G), O1 s (H), and Fe 2p (I) high-resolution XPS spectra of Cur-MPN. (J) TEM image of CM@YM (scale bar, 250 nm). (K) The average hydrodynamic size of the Cur-MPN, YM, and CM@YM. (L) EDS spectra of CM@YM (scale bar, 2 μm). (M) The confocal images of YM and Cur-MPN were labeled by calcium fluorescent white dye (blue) and DiL (red), respectively (scale bar, 2 μm). Data are presented as means ± SD (n = 3).

were placed in EP tubes containing a certain amount of PBS and a 10 % tissue homogenate was made by a high-speed dispersion homogenizer. The mRNA expression and MPO activity in the colon were determined according to the instructions of the RT-qPCR kit and MPO kit.

2.19. Statistical analysis

All the results were statistically analyzed by GraphPad Prism 8.0 software. Student t-test was used for comparison between the two groups. The results were presented as mean ± standard deviation (SD). $P < 0.05$ indicated a statistically significant difference.

3. Results and discussion

3.1. Preparation and characterization of Cur-MPN and CM@YM

The etiology of IBD remains unclear but is generally considered a multifactorial disorder. It involves genetic risk, lifestyle factors, environmental factors, mucosal barrier dysfunction, immune dysregulation, and microbial dysregulation [6,38]. We demonstrated significant differences in the composition of gut flora between IBD patients and the normal population through the GMrepo database [39]. Excluding factors such as age, body mass index (BMI), gender, and region, which may influence gut microorganism composition, patients with IBD display significant differences at the genus level compared to the normal population (Fig. 1A and Table S1). Genera of bacteria essential for nutrient metabolism and intestinal homeostasis, such as Bacteroides and Eubacterium, were found at lower levels than normal in IBD patients, while other pathogenic or potentially pathogenic bacteria were increased. These imbalanced microbiomes not only contribute to chronic inflammation and increased toxicity but also disrupt host metabolism and affect the production of short-chain fatty acids (SCFA) in the gut [40,41]. Inspired by the complex pathogenic mechanism of IBD, we designed a ROS modulator-loaded yeast microcapsule (CM@YM), which could renovate the intestinal microenvironment by relieving inflammation, alleviating oxidative stress, and modulating gut microbiota to effectively ameliorate IBD.

Firstly, a metal polyphenol network (MPN) was prepared by metal coordination between epigallocatechin gallate (EGCG) and Fe^{3+} [34,42]. Curcumin (Cur) was then encapsulated into MPN via self-assembly to form a reticulated structure with a particle size of approximately 321.8 ± 7.12 nm (Fig. 1B and K). The obtained Cur-MPN increased the dispersity of curcumin in water observably (Fig. S1A). UV–vis spectroscopy demonstrated that Cur-MPN had a characteristic absorption peak at 405 nm, confirming the successful encapsulation of curcumin by MPN (Fig. 1C). FTIR spectra revealed characteristic bands associated with curcumin, including C═C and C═O stretching vibrations, C═O and C–C vibrations, and allylic alcohol C–O stretching. The stretching vibration peaks of the phenolic hydroxyl group of EGCG (3360 cm^{-1}) shifted to 3430 cm^{-1}, indicating coordination between Fe^{3+} and EGCG through the partial breaking of hydrogen bonds in the hydroxyl group (Fig. 1D) [43]. Preliminary characterization of the elements contained in Cur-MPN was performed using energy dispersive spectroscopy (EDS) (Fig. S1B), which confirmed the formation of a Fe-based metal polyphenol network. Additionally, X-ray photoelectron spectroscopy (XPS) was conducted to determine the surface elemental content of Cur-MPN, revealing the presence of Fe, C, N, and O (Fig. 1E). HR-XPS spectra showed peak fitting for C 1s, N 1s, O 1s, and Fe 2p, providing detailed information about the chemical bonds present in Cur-MPN (Fig. 1F–I). The binding energy peaks in the HR-C 1s spectrum were assigned to C–C, C–N, C–O, C═O, and O–C═O bonds, while the HR-N 1s spectrum showed peaks corresponding to C–N and -NHx bonds. HR-O 1s spectra indicated the presence of metal oxides, in addition to C–O and C═O bonds, in Cur-MPN. The HR-Fe 2p spectra confirmed the presence of both Fe^{2+} and Fe^{3+} in Cur-MPN.

Next, the yeast microcapsule (YM) with a hollow structure was obtained following previous reports [44]. As shown in Fig. S1C, YM appeared as an elliptical sphere with a diameter of approximately 3 μm. Subsequently, Cur-MPN was further encapsulated into the hollow YM through chemical precipitation with ammonium solution. The particle sizes of YM and CM@YM, as determined by dynamic light scattering (DLS), were 2834.3 ± 189.1 nm and 3102.3 ± 118.8 nm, respectively (Fig. 1K). The particle size of CM@YM was slightly larger than that of YM, indicating the loading of Cur-MPN into the core of YM. The stability of Cur-MPN and CM@YM in an aqueous solution was evaluated for seven days using DLS, and both showed negligible changes in particle size (Figs. S1D and E). The zeta potentials of Cur-MPN and CM@YM were −24.3 ± 0.64 mV and −40.1 ± 0.22 mV, respectively (Fig. S1F), and remained stable within 7 days. This means that negatively charged Cur-MPN and CM@YM are more likely to combine with positively charged inflammatory bowel tissue. Transmission electron microscopy (TEM) and energy-dispersive spectroscopy (EDS) measurements were conducted to confirm the successful encapsulation of Cur-MPN in YM. TEM images revealed high-contrast Cur-MPN nanoparticles in the inner core of YM, indicating the successful encapsulation (Fig. 1J). EDS analysis further confirmed the encapsulation of Cur-MPN in YM by detecting visible iron ions derived from Cur-MPN (Fig. 1L). Fluorescent staining was then used to visually confirm the formation of CM@YM. Calcofluor White, a fluorescent blue dye, was employed to label the wall of YM, while DiL was used as a fluorescent probe to label Cur-MPN. Confocal laser scanning microscopy (CLSM) images showed the typical cystic structure of YM (blue) and the dispersion of Cur-MPN (red) in the nucleus of YM, confirming the successful loading of Cur-MPN into the nucleus of YM (Fig. 1M). The encapsulation efficiency of Cur in Cur-MPN and CM@YM was determined using a modified approach based on previous reports [37]. Both Cur-MPN and CM@YM showed high encapsulation rates, with Cur-MPN at 95.36 ± 1.21% and CM@YM at 67.52 ± 0.73%, demonstrating the effective encapsulation of the drug in the YM-based drug delivery system.

3.2. Stability and antioxidant capacity of CM@YM

The selection of YM as an oral drug carrier for colitis treatment is crucial because it shields the loaded drug from degradation by gastric fluids and facilitates successful release in the intestine. We conducted incubation experiments using YM in simulated gastric fluid (SGF) and simulated intestinal fluid (SIF), and Cur-MPN in SIF and simulated inflammatory colon fluid (SICF). The stability of the microcapsules was assessed through centrifugal collection (Fig. 2A). The morphological changes of YM in aqueous solution, simulated gastric fluid, and simulated intestinal fluid were characterized using scanning electron microscopy (SEM), as presented in Fig. 2B–D. YM exhibited an intact ellipsoidal structure, typical in size with a diameter of approximately 3 μm, both in aqueous solution and simulated gastric fluid, consistent with the TEM results. However, after sequential incubation with simulated gastric and intestinal fluids, the morphology of YM became rough, with fragmented surface structure and exfoliated fragments, consistent with the prior reports [20]. The stability of YM in gastric fluids and its subsequent disintegration in intestinal fluids are instrumental in ensuring the smooth passage of the loaded Cur-MPN through the stomach, facilitating its delivery to the intestinal tract for release.

To further explore the drug release properties of Cur-MPN and CM@YM, the release profiles of Cur-MPN and CM@YM were evaluated in SGF, SIF, and the presence of 0.5% β-glucanase enzymes in SIF. As shown in Fig. S2, compared with CM@YM, Cur-MPN showed faster release among SGF, and SIF solution with significant differences, which indicated that YM showed a longer-lasting sustained-release effect to curcumin and EGCG release both in gastric and intestinal environments. Interestingly, under the condition of 0.5% β-glucanase, the release behavior of curcumin and EGCG from CM@YM was faster than without β-glucanase. Suggestively, CM@YM was sensitive to β-glucanase due to the β-glucan involved on the YM surface. The aforementioned results

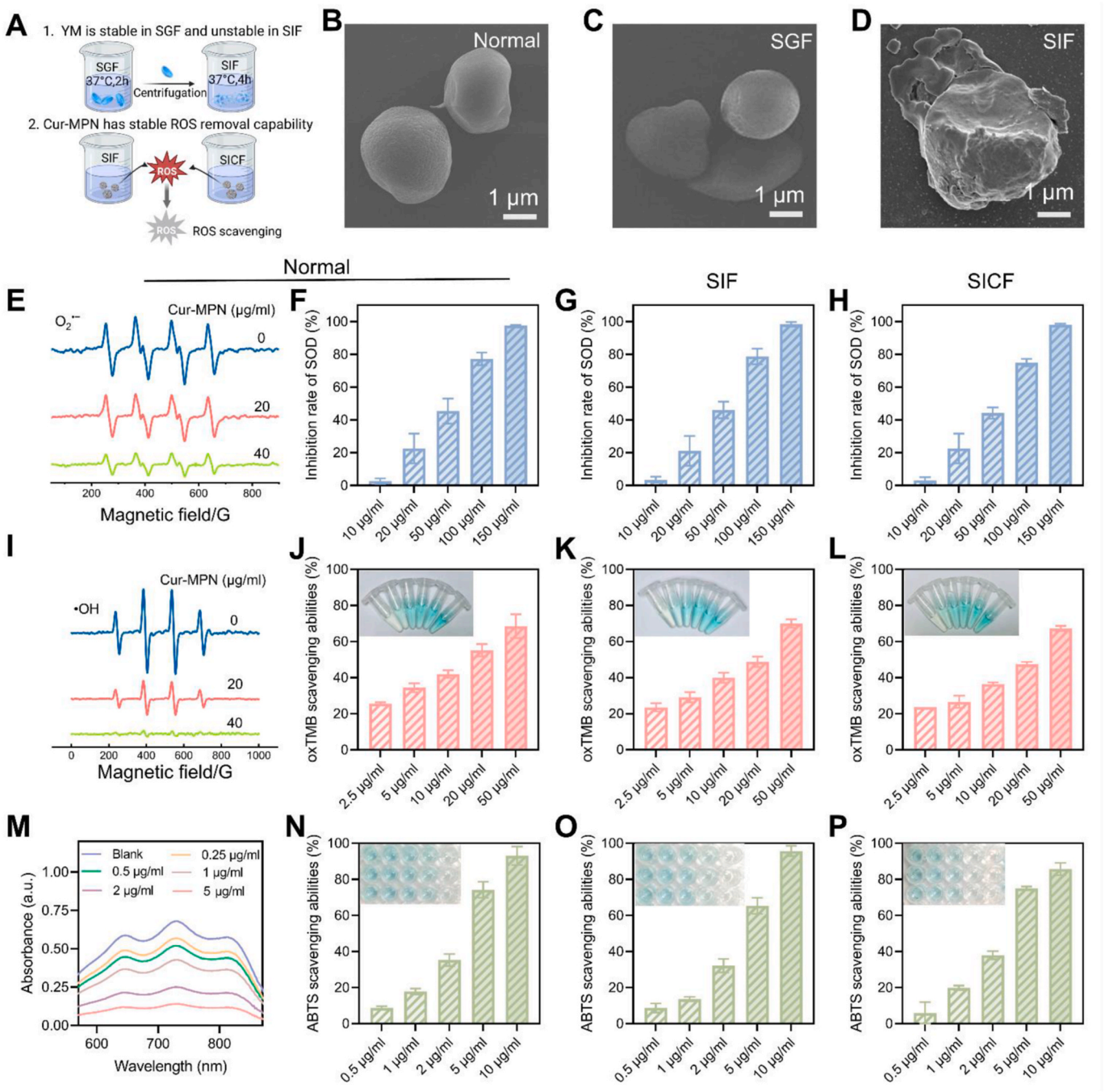

Fig. 2. Stability and antioxidant capacity of CM@YM. (A) The schematic shows the stability of YM in SGF and the stable ROS scavenging ability of Cur-MPN. (B–D) SEM characterization of YM incubated in the normal environment, SGF, and SIF (scale bar, 1 μm). (E) $O_2^{\bullet-}$ scavenging ability of Cur-MPN detected by BMPO. (F–H) Percentage of superoxide radical elimination catalyzed by SOD-like activity of Cur-MPN in the normal environment, SIF, and SICF. (I) ·OH scavenging ability of Cur-MPN detected by DMPO. (J–L) The quantitative analysis of oxTMB scavenging rate by Cur-MPN at different concentrations (2.5, 5, 10, 20, and 50 μg/mL) in the normal environment, SIF, and SICF (insert, a photograph of the above-mentioned solutions after reaction). (M) UV–vis absorbance spectra of ABTS+• radical after incubation with different concentrations Cur-MPN (0.25, 0.5, 1, 2, and 5 μg/mL). (N–P) The quantitative analysis of ABTS+• scavenging rate by Cur-MPN at different concentrations (0.5, 1, 2, 5, and 10 μg/mL) in the normal environment, SIF, and SICF (insert, a photograph of the above-mentioned solutions after reaction). Data are presented as means ± SD (n = 3).

indicated that CM@YM may achieve targeted release under the influence of 0.5% β-glucanase produced by the intestinal flora [45], which is a good oral delivery system for IBD.

In the progression of IBD, highly expressed ROS causes biomolecular damages such as lipid peroxidation, DNA damage, and protein denaturation, leading to elevated oxidative stress and excessive inflammatory responses [46–48]. Therefore, the elimination of excess ROS is crucial for IBD treatment. Moreover, the intestinal fluid is typically weakly alkaline and contains various enzymes involved in food digestion, which might impact the activity of nanoparticles upon reaching the intestine. After CM@YM enters the intestine, the loaded Cur-MPN is released and exhibits its therapeutic effects through YM disintegration in the intestinal fluid. To validate the efficacy of Cur-MPN in scavenging ROS in inflammatory bowel, we conducted comprehensive evaluations

of Cur-MPN scavenging and total antioxidant capacity against three representative ROS: superoxide radicals, hydroxyl radicals, and hydrogen peroxide. These evaluations were performed in normal pH, SIF, and SICF.

In this experiment, electron spin resonance (ESR) was utilized to assess the ability of Cur-MPN to scavenge the $O_2^{\bullet-}$ radical. To generate $O_2^{\bullet-}$, the hypoxanthine/xanthine oxidase (HYP/XOD) system was employed. 5-tert-Butoxycarbonyl-5-methyl-1-pyrroline-N-oxide (BMPO) was then added as a trapping agent to capture $O_2^{\bullet-}$ and form a spin adduct called BMPO/·OOH. The signal intensity of the ESR spectra was measured to analyze the scavenging capability of Cur-MPN. When both BMPO and $O_2^{\bullet-}$ were present, a distinct signal peak appeared, indicating the successful capture of $O_2^{\bullet-}$ by BMPO. However, as the concentration of Cur-MPN increased, the intensity of the signal peak decreased significantly. This observation suggests that Cur-MPN possesses excellent $O_2^{\bullet-}$ scavenging ability (Fig. 2E). Furthermore, the commercial kits were used to assess the superoxide dismutase (SOD) enzyme activity and stability of Cur-MPN in different environments (Fig. 2F–H). The results revealed that Cur-MPN exhibited a robust SOD enzyme-like activity. Notably, this strong enzyme activity remained stable in SIF and SICF. Overall, these findings demonstrate the potent $O_2^{\bullet-}$ scavenging ability of Cur-MPN and its stability under different conditions, indicating its potential as a therapeutic agent for oxidative stress-related disorders.

In addition to $O_2^{\bullet-}$, hydroxyl radical (·OH) is another ROS that possesses potent oxidizing properties. Effective removal of ·OH is crucial in preventing cellular damage caused by ROS. To evaluate the scavenging effect of Cur-MPN on ·OH, we employed the Fenton reaction (Fe^{2+}/H_2O_2) to generate ·OH. 5,5-Dimethyl-1-pyrroline N-oxide (DMPO) was used to capture ·OH and form spin adducts called DMPO/·OH. The change in ESR signal intensity was employed to assess the scavenging effect of ·OH. In the absence of Cur-MPN, the ESR spectra exhibited characteristic four-linear (1:2:2:1) peaks attributed to ·OH (Fig. 2I). However, upon the addition of Cur-MPN, the signal intensity of the characteristic four-linear peaks decreased. At 40 μg/mL, the signal almost disappeared, indicating the high ·OH removal ability of Cur-MPN. These findings confirm the excellent ·OH scavenging ability of MPN. Furthermore, we utilized 3,3,5,5-tetramethylbenzidine (TMB), which can be oxidized by ·OH and turns blue, as an indicator to assess the ·OH scavenging ability of Cur-MPN in various environments. The blue color of the reaction system faded when Cur-MPN incubated with different environments, indicating that the ·OH scavenging ability of Cur-MPN remained stable in the intestinal environment (Fig. 2J-L). Additionally, the absorption peak of oxidized TMB (oxTMB) at 650 nm decreased as the concentration of Cur-MPN increased, as measured by a UV spectrophotometer (Fig. S3A). The use of a terephthalic acid (TA) fluorescent probe, another ·OH indicator, also confirmed the excellent ·OH scavenging performance of Cur-MPN (Fig. S3B). Overall, these results highlight the exceptional ·OH scavenging ability of Cur-MPN, indicating its potential as a therapeutic agent for protecting cells against oxidative damage caused by ROS.

After incubation with different concentrations of H_2O_2 (0.6, 1.2, 2.5, and 5 mM), the color of Cur-MPN gradually became lighter, indicating its reactivity and scavenging ability towards H_2O_2 (Fig. S3C). To further assess the total antioxidant capacity of Cur-MPN, we used the 2,2-azino-bis(3-ethylbenzothiazoline-6-sulfonic acid) radical (ABTS+•) assay. In a stable condition, ABTS+• appears as a blue-green color with a maximum absorption peak at 734 nm. By employing the ABTS method, we examined the total antioxidant capacity of Cur-MPN and its stability (Fig. 2M − P). The results showed the excellent antioxidant capacity of Cur-MPN. Collectively, these findings demonstrate that CM@YM is capable of traversing the harsh environment of the stomach and subsequently releasing the drug in the intestine. The released Cur-MPN effectively scavenges the highly expressed ROS in IBD and remains stable in the intestinal environment. This endows Cur-MPN a promising therapeutic agent for the treatment of colitis.

3.3. The uptake of CM@YM in living cells

Macrophages are known to play a crucial role in the development and progression of IBD [49,50]. Targeted regulation of intestinal macrophages is therefore an important approach to managing IBD. Considering the presence of β-glucan on the surface of YM, we hypothesized that CM@YM could be specifically recognized by the dectin-1 receptor on macrophages, thereby effectively targeting macrophages in the intestinal system. To investigate this hypothesis, we examined the uptake ability of macrophages to Cur-MPN and CM@YM. To better observe the binding effect of nanoparticles in RAW 264.7 cells, the sample of Cur-MPN and CM@YM was labeled with DiL. As shown in Fig. 3A, after 4 h of incubation, the uptake of CM@YM was significantly higher in RAW 264.7 cells compared to Cur-MPN. Conversely, after pretreatment of RAW 264.7 cells with laminarin, a dectin-1 inhibitor, the CLSM image of the CM@YM group showed no obvious red fluorescence, while the Cur-MPN group showed almost no change, which was consistent with the results of flow cytometry (Fig. 3B). Continued study of CM@YM binding to the dectin-1 receptor using dectin-1 barely expressing FHC cells as a control. As shown in Fig. 3A, the uptake efficiency of Cur-MPN and CM@YM by FHC cells was completely different from that of RAW 264.7 cells. FHC cells showed a higher uptake efficiency for Cur-MPN, probably because Cur-MPN is more advantageously sized to be taken up by the cells. However, this remained unchanged in the case of early incubation with dectin-1 receptor inhibitors, which was consistent with the results of flow cytometry (Fig. 3C). These results suggest that CM@YM can effectively target RAW 264.7 cells and that it is critical that YM binds to the dectin-1 receptor on the surface of RAW 264.7 cells.

Mitochondria are the main organelles in the cells that produce ROS, we tested if CM@YM is co-located with mitochondria to scavenge ROS after being internalized by the cells. The fluorescence images showed that CM@YM labeled by DiL was co-localized with the mitochondria (Fig. 3D). Nevertheless, mitochondria were not the only accumulation sites of the nanoparticles. CM@YM was also partially colocalized with Lyso-tracker Green, supposing that CM@YM was partially trapped in lysosomes (Fig. 3G). Both Pearson's colocalization coefficient (PCC) and Manders' co-localization coefficients (MCC) were measured to determine the co-localization of DiL fluorescence signals with Mito-tracker Green or Lyso-tracker Green. It was found that PCC was 0.95 for mitochondria and 0.96 for lysosome co-localization with CM@YM (Fig. 3E and H), indicating CM@YM colocalized with both mitochondria and lysosomes to some extent. MCC results were consistent with PCC. Additionally, the plot profile analysis further supported the results of PCC and MCC analyses. The red peaks indicating CM@YM and the green peaks indicating Mito-tracker Green or Lyso-tracker Green presented a certain correlation, suggesting partly co-localization (Fig. 3F and I). In summary, CM@YM is not only co-localized with mitochondria but also partially co-localized with lysosomes.

3.4. Anti-oxidant and anti-inflammatory effects of Cur-MPN and CM@YM in living cells

Since oxidative stress induced by excess ROS production can lead to lipid peroxidation, protein damage, and DNA breakage, the intracellular ROS scavenging properties of Cur-MPN and CM@YM were investigated by a 2,7-dichlorofluorescein diacetate (DCFH-DA) probe and dihydroethidium (DHE) probe. The results, shown in Fig. 3J and K, indicated that the H_2O_2-induced group exhibited a strong green fluorescence of DCF and red fluorescence of DHE compared to the blank group, indicating successful induction of ROS production by H_2O_2. However, the fluorescence intensity of DCF and DHE significantly attenuated when cells were pre-incubated with Cur-MPN or CM@YM, indicating that both Cur-MPN and CM@YM effectively reduced the ROS content in H_2O_2-induced cells. Subsequently, the protection mechanism of Cur-MPN and CM@YM for H_2O_2-induced RAW 264.7 apoptosis was evaluated. Calcein AM/propidium iodide (AM/PI) staining of H_2O_2-treated RAW 264.7

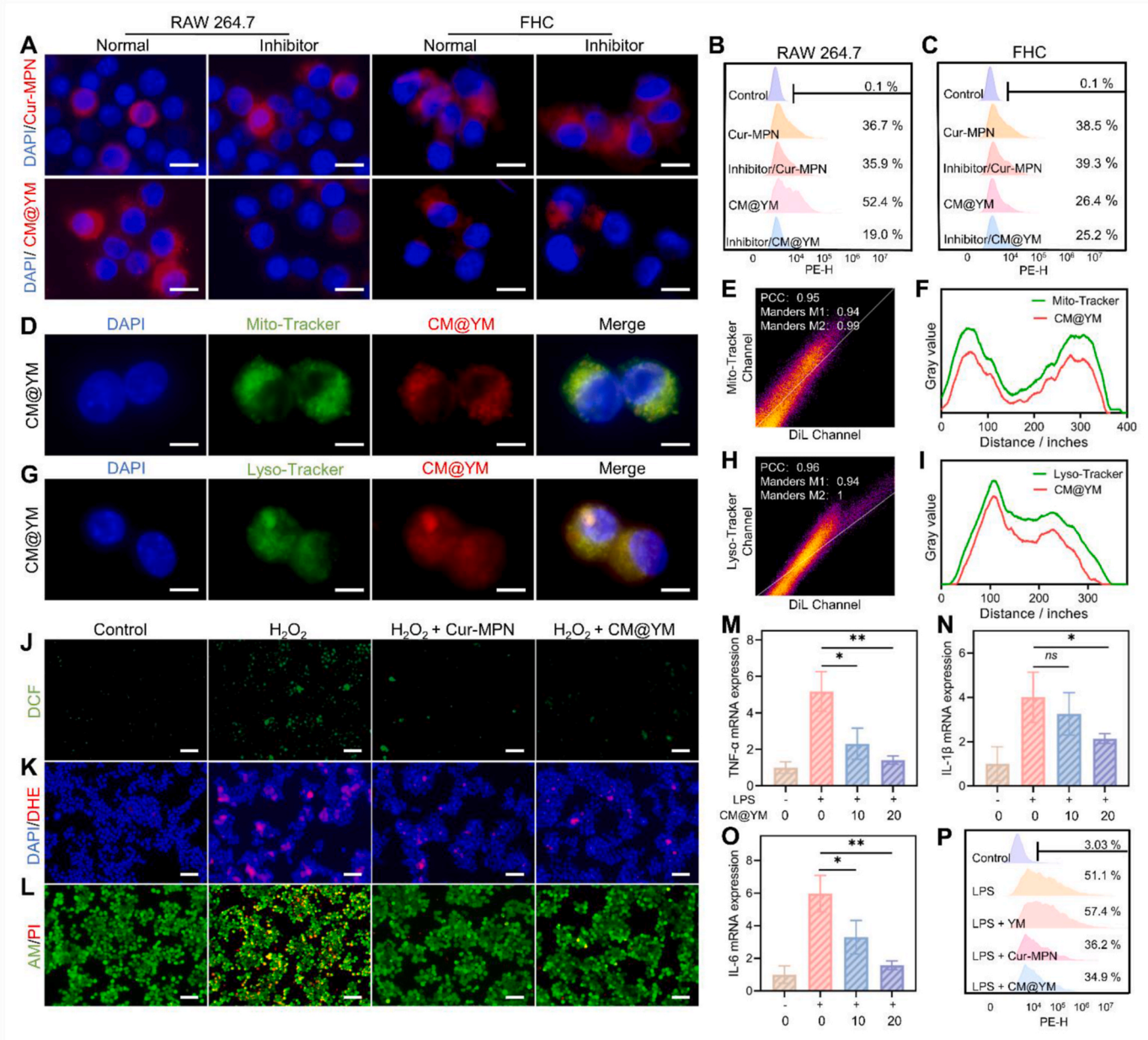

Fig. 3. The cellular internalization and anti-oxidant and anti-inflammatory effects of Cur-MPN and CM@YM. (A) Cellular uptake of Cur-MPN and CM@YM in RAW 264.7 and FHC cells (scale bar, 20 μm). Intracellular CM@YM fluorescence in RAW 264.7 (B) and FHC (C) cells was detected by flow cytometry. Co-localization fluorescence images of CM@YM and mitochondria (D) and lysosomes (G) (scale bar, 10 μm). The PCC (Pearson's correlation coefficient) and MCC (Mander's correlation coefficients) analysis of CM@YM with mitochondria (E) or lysosomes (H). The plot profile analysis of CM@YM with mitochondria (F) or lysosomes (I). Typical fluorescence images of RAW 264.7 cells stained with DCFH-DA (J), DAPI/DHE (K), and AM/PI (L) after various treatments (scale bar, 50 μm). The mRNA expression levels of TNF-α (M), IL-1β (N), and IL-6 (O) in RAW 264.7 cells. (P) Flow cytometric examination of the M1-phenotype macrophages in different groups. Data are presented as means ± SD (n = 3; *P < 0.05, **P < 0.01).

showed a red signal indicative of dead cells. However, the red signal significantly decreased upon treatment with Cur-MPN and CM@YM, indicating that Cur-MPN and CM@YM could scavenge H_2O_2 and block H_2O_2-induced cell apoptosis (Fig. 3L). Furthermore, as revealed by the MTT assay, H_2O_2 treatment could amplify the intracellular oxidative stress and eventually cause RAW 264.7 apoptosis (Fig. S4). In contrast, pretreatment of Cur-MPN and CM@YM could significantly relieve oxidative stress and abolish cell apoptosis, indicating that almost all of H_2O_2 was scavenged by Cur-MPN and CM@YM.

After confirming the ability of CM@YM to scavenge excessive intracellular ROS and inhibit oxidative damage, it was further investigated whether CM@YM could inhibit inflammation induced by LPS in RAW 264.7 cells. The results, shown in Fig. S5A, indicated that the LPS-induced group exhibited a strong green fluorescence of DCF compared to the blank group, indicating successful induction of ROS production by LPS. However, the green fluorescence intensity of DCF significantly attenuated when cells were pre-incubated with Cur-MPN or CM@YM, indicating that both Cur-MPN and CM@YM effectively reduced the ROS content in LPS-induced cells. The fluorescence content of DCF in RAW 264.7 cells was quantified using flow cytometry (Fig. S5B). LPS treatment led to the upregulation of pro-inflammatory cytokines TNF-α, IL-1β, and IL-6. However, pre-treatment with CM@YM in RAW 264.7 cells resulted in the reduction of these pro-inflammatory cytokine levels (Fig. 3M – O), indicating the significant anti-inflammatory capacity of CM@YM.

In addition to the ability to alleviate inflammation by inhibiting ROS

production, changes in macrophage phenotype were also closely associated with the inflammatory disease process. Macrophages can be categorized into two subpopulations, namely M1 and M2, with M1 macrophages being pro-inflammatory cells that are involved in host defense against bacteria and viral infections [51]. The overexpression of surface markers such as CD80, CD86, and CD16/32 can be used to identify M1 macrophages. Since the phenotype of macrophages plays a crucial role in inflammation, we proceeded to investigate whether CM@YM could effectively modulate macrophage phenotype by examining the expression level of the M1 macrophage surface marker CD86. LPS-induced M1 macrophages were incubated with a specific amount of YM, Cur-MPN, and CM@YM for 24 h. The expression of CD86 on RAW 264.7 cells was then assessed using flow cytometry. As shown in Fig. 3P, the expression of CD86 increased significantly after LPS induction. Interestingly, while YM treatment did not reduce the expression of CD86, it led to a slight increase in CD86 expression. This may be attributed to the biologically active components on the surface of YM, such as polysaccharides, stimulating a stress response in macrophages. In contrast, both the Cur-MPN and CM@YM groups exhibited successful modulation of macrophage phenotype, resulting in a significant reduction in CD86 expression in macrophage cells. To better visualize the reprogramming ability of Cur-MPN and CM@YM on macrophages, we

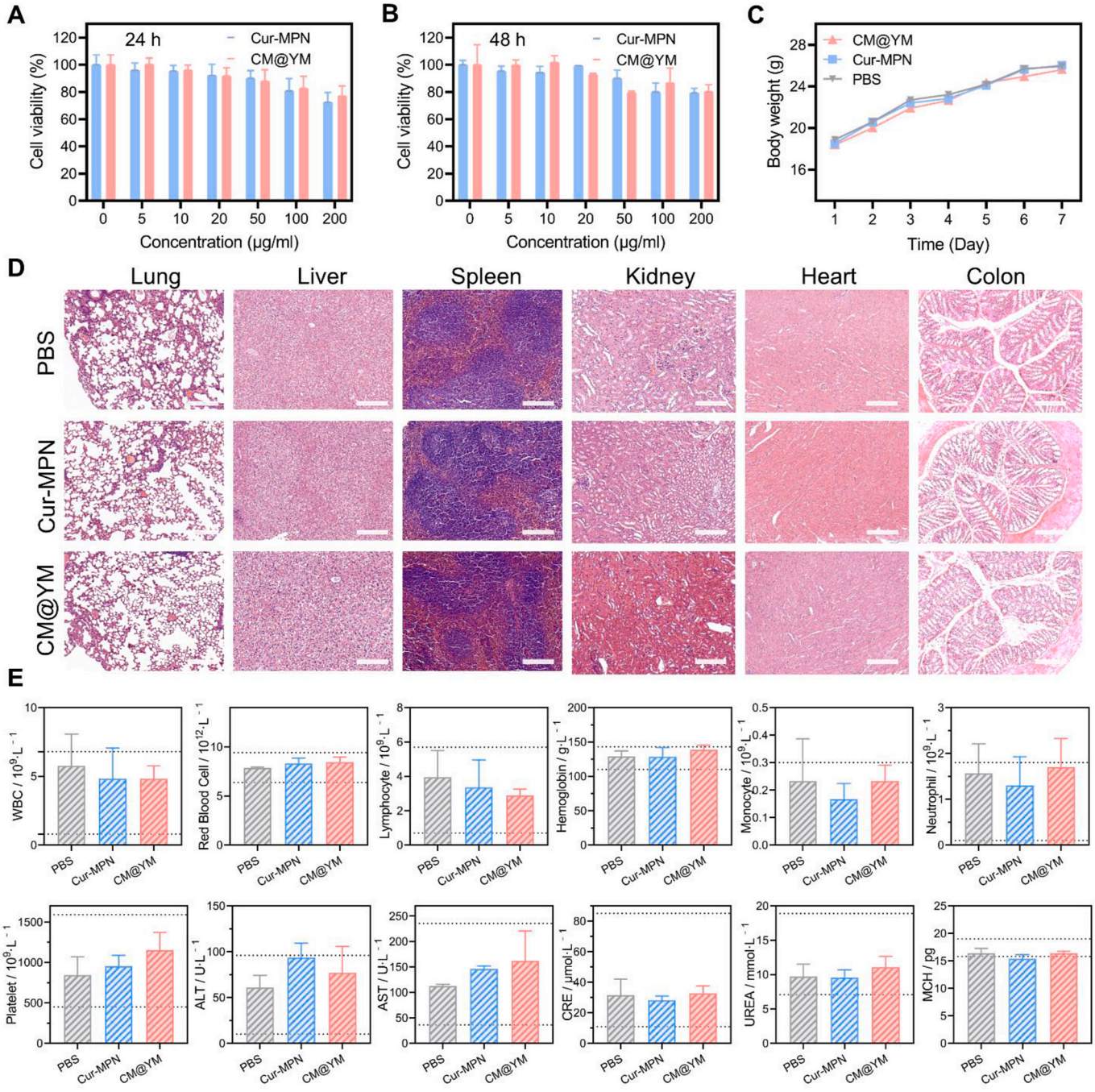

Fig. 4. Biocompatibility evaluation of Cur-MPN and CM@YM. (A–B) Relative viabilities of RAW 264.7 cells after incubation with different concentrations of Cur-MPN and CM@YM (5, 10, 20, 50, 100, and 200 μg/mL) for 24 h and 48 h. (C) Body weight changes of mice within 7 days after oral administration of Cur-MPN and CM@YM. (D) H&E staining for vital organs was used to assess the systemic toxicity of Cur-MPN and CM@YM (scale bar, 100 μm). (E) Complete blood panel analysis results and blood biochemistry analysis results for treated mice. Data are presented as means ± SD (n = 3).

recorded morphological changes on RAW 264.7 cells by microscopy. Through the microscope recording, it could be seen that the cell morphology of the control group showed circular growth, while the cell morphology of the LPS group was varied, and the round cells were significantly reduced. Approximately 90% of the cells in the LPS-treated group showed dendritic, radial, or long spindle shapes, similar to the morphology of M1 macrophages. On the contrary, the cell morphology of the LPS + Cur-MPN group and LPS + CM@YM group was round, indicating that the cell polarization was inhibited (Fig. S5C). Based on our findings, it can be concluded that CM@YM effectively inhibits the

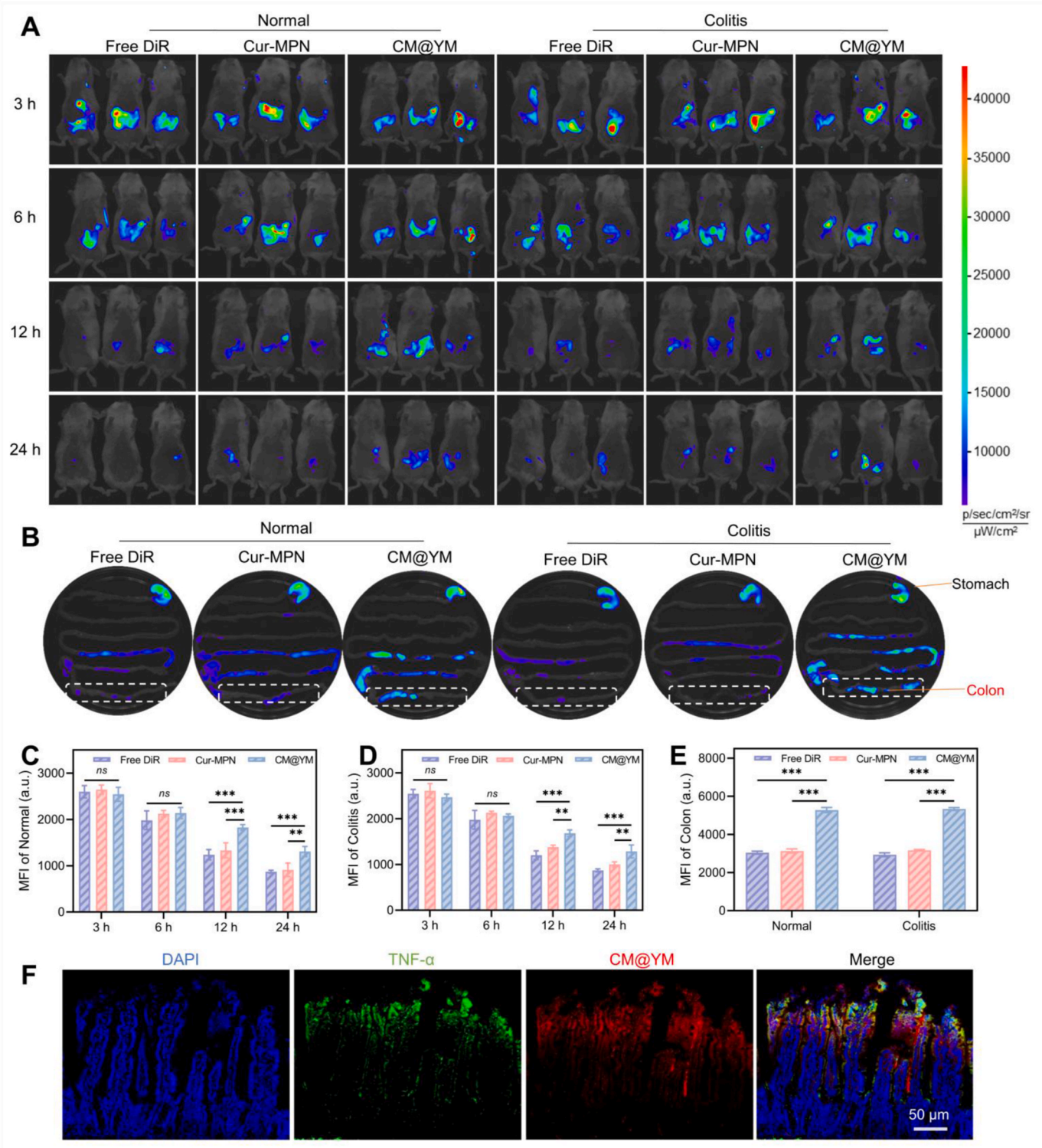

Fig. 5. The targeting and retention abilities of CM@YM to the inflamed colon. (A) *In vivo* fluorescence images of normal and colitis mice at different time points after oral administration of different preparations. (B) Fluorescence images of mice cecum-colon tissues at the endpoint. (C) Histogram of normal mice at different time points after oral administration of different preparations. (D) Histogram of colitis mice at different time points after oral administration of different preparations. (E) Fluorescence histogram of mice colon at the endpoint. (F) Immunofluorescence staining of colon tissue from colitis mice incubated with CM@YM for 6 h (scale bar, 50 μm). Data are presented as means ± SD (n = 3; **P < 0.01, ***P < 0.001).

M1 polarization of macrophages when stimulated by LPS, thereby achieving the desired anti-inflammatory effect, and this function is attributed to the presence of Cur-MPN in CM@YM.

Overall, these findings demonstrate that Cur-MPN and CM@YM effectively scavenge intracellular ROS, inhibit inflammation, and regulate the polarization of macrophagesprotect in RAW 264.7 cells. This highlights the potential of CM@YM as a therapeutic agent for anti-inflammatory and antioxidant interventions.

3.5. Biocompatibility evaluation of Cur-MPN and CM@YM

Biocompatibility was systematically assessed to ensure the safety of CM@YM for oral administration. The biocompatibility of Cur-MPN and CM@YM was initially investigated using the MTT assay. As shown in Fig. 4A and B, the cell viability of RAW 264.7 cells did not exhibit any significant decrease after 24 and 48 h of co-incubation with Cur-MPN or CM@YM, with a decreasing trend observed only at the highest concentration of 200 μg/mL suggesting that both Cur-MPN and CM@YM have excellent biocompatibility. In FHC cells, the biocompatibility of Cur-MPN and CM@YM was equally excellent (Fig. S6). We further evaluate the biocompatibility in vivo. The body weight changes of the mice were recorded after oral administration of Cur-MPN or CM@YM (40 mg/kg) for seven days. As shown in Fig. 4C, there was no significant difference in body weight among the three groups of mice during the entire experimental period. To assess the potential toxicity of CM@YM, we performed histological evaluation of vital organs using H&E staining. Fig. 4D showed that there were no observable histological changes or cellular destruction in the vital organs of the mice treated with Cur-MPN or CM@YM compared to the healthy mice. Moreover, we analyzed routine blood indices and blood biochemical indices of the mice treated with Cur-MPN or CM@YM and found no significant differences compared to the healthy mice (Fig. 4E). All these results indicate that CM@YM exhibits excellent biocompatibility and can be used for in vivo experiments.

3.6. The targeting and retention abilities of CM@YM to the inflamed colon

Targeting the inflamed site in the intestine through oral administration is an effective and straightforward delivery strategy for treating UC. However, for this strategy to be successful, it is crucial for the oral delivery system to effectively target and retain at the site of inflammation for an extended period. YM, a natural microencapsulation carrier, is particularly suitable for this purpose due to its enrichment with β 1,3-D-glucan on its surface, which enables it to target macrophages and inflammation. Additionally, the presence of polysaccharides and the uneven structure on the surface of YM allow for longer retention in the intestinal tract. To demonstrate the targeting and retention ability of CM@YM microcapsules at the site of intestinal inflammation, we conducted a series of experiments using a small animal in vivo imaging system. DiR-labeled delivery systems were prepared (at a dose of 0.75 mg/kg DiR) and the distribution of the microcapsules in mice was investigated by performing in vivo fluorescence imaging at 3, 6, 12 and 24 h after oral administration and ex vivo fluorescence imaging of the gastrointestinal tract of mice at the endpoint. As shown in Fig. 5A and B, under the same administration conditions, Free DiR and Cur-MPN had the shortest residence time in the gastrointestinal tract and the fastest disappearance of fluorescence. After 12 h of oral administration, the fluorescent signals of Free DiR and Cur-MPN became extremely weak in mice. However, CM@YM microcapsules retained their fluorescence at the intestinal site even after 24 h (Fig. 5E). The fluorescence histogram showed that there was no significant difference in the average fluorescence intensity of Free DiR, Cur-MPN, and CM@YM groups after 3 and 6 h of oral administration. After 12 h, the average fluorescence intensity of CM@YM was stronger than that of the other three groups with a significant difference ($p < 0.01$), which continued to the terminal point (Fig. 5C). We further investigated the retention effect of CM@YM in colitis mice (Fig. 5A, B, and D). The results were similar to those of normal mice, with CM@YM demonstrating a very superior retention effect and retaining slightly more area in the inflamed colon than in the normal colon. This initial evidence corroborates the targeting effect of the microcapsules on the inflamed intestinal tract. Overall, these findings demonstrate the ability of CM@YM microcapsules to effectively target and retain at the site of intestinal inflammation, making them a promising therapeutic approach for the treatment of UC.

To investigate the retention of CM@YM in the inflamed intestines of colitis mice at a microscopic level, we collected colonic segments from colitis mice after 6 h of CM@YM gavage administration and performed immunofluorescence staining of TNF-α. As shown in Fig. 5F, the green fluorescence representing TNF-α was prominently expressed in the colonic site, indicating the presence of inflammation. Additionally, the red fluorescence representing CM@YM was found to be concentrated in the interstitial space of the intestinal villi and primarily localized in the mucus layer. This observation confirms that the YM encapsulation enables CM@YM to specifically target the inflamed intestine and remain there for an extended period. This microscopic analysis provides further evidence that CM@YM can effectively target and retain at the site of inflammation in the intestines, enhancing its therapeutic potential for the treatment of ulcerative colitis.

3.7. Protective effect of CM@YM against DSS-induced colitis

To assess the protective effect of CM@YM against DSS-induced acute colitis, we conducted a comprehensive evaluation using various parameters. All C57 mice were randomly divided into five groups: blank control, DSS model, YM, Cur-MPN, and CM@YM groups. Except for the control group, each group received 2.5% DSS in their drinking water to induce colitis. The corresponding treatments (YM, Cur-MPN, or CM@YM) were administered by gavage every other day for a total of six times. At the end of the experiment, the colon was collected after euthanization (Fig. 6A). The protective effect was assessed through several measures, including changes in body weight of the mice, disease activity index (DAI), colon length differences, myeloperoxidase (MPO) content, analysis of cytokine levels and molecular markers of oxidative stress, and histological examination of inflammation. By monitoring changes in body weight, DAI, and colon length, we can gauge the overall impact of the treatments on the mice. MPO content, which is an indicator of inflammation, was measured in the colonic tissue samples. Furthermore, we analyzed the levels of cytokines to determine the inflammatory response, as well as the molecular markers of oxidative stress to assess the antioxidant effects. Finally, histological examinations were performed to evaluate the extent of inflammation. These comprehensive evaluations will provide valuable insights into the therapeutic efficacy of CM@YM in alleviating DSS-induced acute colitis in mice.

In Fig. 6B and C, it was observed that the control group of mice experienced continuous weight gain and showed no changes in the DAI score, indicating their normal state of growth. Conversely, mice in the model group exhibited significant and continuous weight loss starting from day 5, and the DAI index also steadily increased. However, in the other three treatment groups (YM, Cur-MPN, and CM@YM), the weight loss and rise in the DAI index were inhibited to varying degrees. Notably, the CM@YM group demonstrated the most effective inhibition, indicating its superior protective effect. To further assess the progression of colitis, we analyzed the colon length, spleen index, endoscopic changes, and histological alterations in the mice (Fig. 6D–H). The colon length in the model group was significantly shortened from 8.53 ± 0.41 cm to 4.10 ± 0.082 cm, indicating successful colitis induction. However, the CM@YM group exhibited a protective effect superior to both the YM and Cur-MPN groups, with the colon length restored to 6.40 ± 0.22 cm. In addition, the spleen was the site of immune cell settlement, and changes in the spleen were also evident after the execution of the mice. The

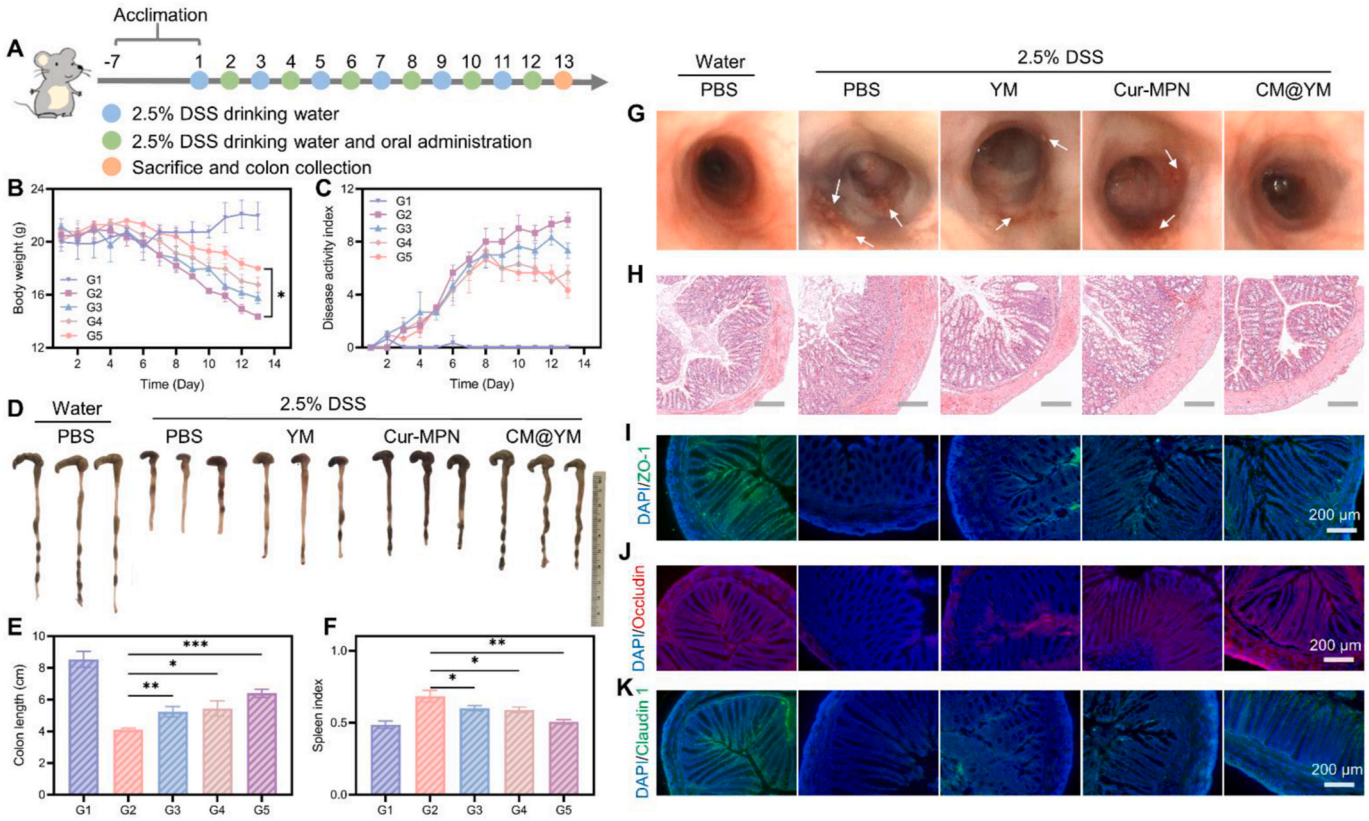

Fig. 6. Protective effect of CM@YM against DSS-induced colitis. (A) Schematic showing the experimental procedure for the treatment of DSS-induced colitis mice. (B) Daily body weight over 13 days. (C) DAI score of colitis model mice during the experiment. (D) Photographs of the excised colons from the colitis models on day 13 after treatment. (E) Measurements of colon lengths after different treatments. (F) Measurements of spleen index after different treatments. (G) Representative photos of the intestinal endoscope of mice treated with the indicated materials on day 13. (H) H&E staining of colonic pathological sections of mice treated with the indicated materials on day 13 (scale bar, 200 μm). Immunofluorescence image of ZO-1 (I), occludin (J), and claudin-1 (K) in the colons (scale bar, 200 μm). G1: control group, G2: DSS group, G3: DSS + YM group, G4: DSS + Cur-MPN group, G5: DSS + CM@YM group. Data are presented as means ± SD (n = 5; *P < 0.05, **P < 0.01, ***P < 0.001).

spleen was significantly restored after CM@YM treatment compared to the no-drug groups (Fig. S7). In terms of endoscopic findings, the model group showed structural rigidity of the intestinal lumen with prominent ulcerative lesions. The YM group showed poorer efficacy, with multiple ulcerative lesions in the colon. In contrast, both the Cur-MPN and CM@YM groups exhibited superior efficacy, with red and moist intestinal mucosa and preserved structural integrity, with fewer or no ulcers present. The histological evaluation through H&E staining revealed that the colon sections of normal mice showed no significant inflammatory areas. However, the colon sections of mice in the model group exhibited distinct inflammatory features, including colonic epithelial thickening, inflammatory cell aggregation and infiltration, structural incompleteness, and cryptgland rupture. Comparing the YM and Cur-MPN groups with the model group, we observed a slight reduction in the severity of colitis. Notably, the colon sections from CM@YM-treated mice displayed a significant restoration of the mucosal layer structure. The abundance of cup cells in the crypts resembled that of the normal control group, indicating a substantial recovery of the colonic epithelium and a significant reduction in inflammation. In summary, these results strongly support the excellent protective effect of CM@YM in DSS-induced acute colitis.

To assess the integrity of the colonic mucosal barrier, we examined the expression levels of tight junction-associated proteins, including ZO-1, Occludin, and Claudin-1, in colonic tissues. Immunofluorescence staining revealed that the colonic tissues of CM@YM-treated mice exhibited significant enrichment of ZO-1, Occludin, and Claudin-1 (Fig. 6I–K). These findings indicate that CM@YM treatment effectively restored the integrity of the intestinal mucosal barrier in colitis mice.

3.8. Anti-oxidant and anti-inflammatory effects of CM@YM microcapsule in vivo

To visualize the inflammation level in the intestines, immunofluorescence analysis was performed on the retained colon tissues. DCFH-DA and DHE were used to label ROS in the colon tissues. As shown in Fig. 7A and B, the model and YM groups exhibited intense red fluorescence, indicating high inflammation, while the Cur-MPN and CM@YM groups showed minimal expression of red fluorescence, suggesting reduced inflammation. Furthermore, to gain further insights into the regulatory effect of CM@YM on macrophage phenotype in the mouse colon, we conducted an analysis of macrophage phenotype in the colon by labeling CD86 and CD206 markers (Fig. 7C and D). Comparing the Cur-MPN group with the CM@YM group, it was observed that the model and YM groups exhibited a significant increase in CD86 signal and a significant decrease in CD206 signal. These findings suggest that the ability of CM@YM to scavenge ROS and regulate macrophage polarization phenotypes is mainly derived from Cur-MPN. While both YM and Cur-MPN showed indistinctive protective effects on DSS-induced colitis, the core-shell structure of CM@YM significantly enhanced the protective effects. This enhancement can be attributed to the adhesion and inflammatory targeting of YM to the mucus layer, which improved the retention time of Cur-MPN in the inflamed intestine. The anti-inflammatory effect of CM@YM was further demonstrated by measuring the expression of pro-inflammatory cytokines (TNF-α, IL-6, IL-1β) in colon homogenates using qRT-PCR. As depicted in Fig. 7E–G, the expression levels of TNF-α, IL-6, and IL-1β were significantly reduced after the application of CM@YM, indicating its anti-inflammatory properties. This effect was also

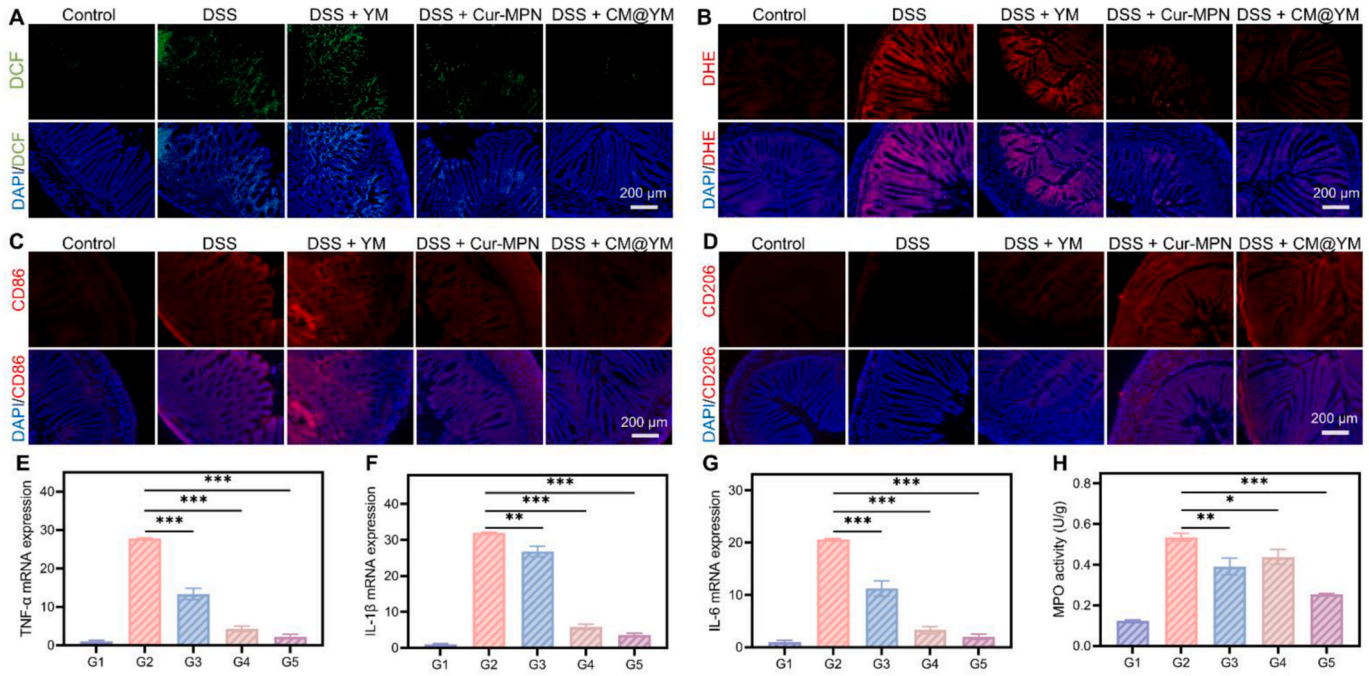

Fig. 7. Anti-oxidant and anti-inflammatory effects of CM@YM. Immunofluorescence image of DCFH-DA (A), DHE (B), CD86 (C), and CD206 (D) in the colons (scale bar, 200 μm). The levels of mRNA expression of TNF-α (E), IL-1β (F), and IL-6 (G) in colon tissues. (H) MPO activity in colon tissues. G1: control group, G2: DSS group, G3: DSS + YM group, G4: DSS + Cur-MPN group, G5: DSS + CM@YM group. Data are presented as means ± SD (n = 5; *P < 0.05, **P < 0.01, ***P < 0.001).

supported by the lower levels of MPO content in colon homogenates in CM@YM-treated mice, compared to the model group (Fig. 7H).

3.9. Modulating gut microbiota by CM@YM

The gut microbiota plays an important role in the regulation of host metabolism, immunity, and intestinal barrier function. We collected feces from mice and performed 16S rRNA gene sequencing to analyze the overall structure of the intestinal microbiota. Species accumulation curves indicate that the sample size is sufficient to reflect the species composition of the community (Fig. S8A). Alpha-diversity analysis, as determined by Chao1 and Shannon's Diversity Index, showed that the bacterial diversity in the DSS group was significantly lower compared to the control group. However, the bacterial diversity in the CM@YM group was not significantly different from the control group (Fig. 8A and B). Principal coordinate analysis (PCoA) was conducted to assess beta diversity and revealed that mice in the DSS group had a distinct gut microbial profile compared to the control group. In contrast, the gut microbiota of the CM@YM group was more similar to that of the control group (Fig. 8C). The composition of the gut microbiota at the phylum level, as shown in Fig. 8D, demonstrated that DSS treatment significantly reduced the content of Firmicutes and increased the content of Proteobacteria when compared to the control group. However, the CM@YM group exhibited a gut microbiota composition at the phylum level that was closer to the control group. Similar results were observed at the class level (Fig. S8B). Visualizing the species composition of the samples at each taxonomic level, taxonomic branching plots of LEfSe were generated (Fig. 8E). The heat map depicted the relative abundance of gut microbiota at the genus level for the different groups (Fig. 8F). In the DSS group, the relative abundance of pathogenic or conditionally pathogenic bacteria, such as *Pseudomonas*, *Bilophila*, *Enterococcus*, and *Shigella*, increased. In contrast, the CM@YM group exhibited an increased relative abundance of probiotic bacteria, including *Akkermansia*, *Faecalibacterium*, and *Coprococcus*. In the normal group of mice, the three most abundant bacteria at the genus level were *Akkermansia*, *Allobaculum*, and *Turicibacter*. However, the administration of DSS caused a significant change in the composition of the gut microbiota, which was effectively restored by the treatment of CM@YM (Fig. 8G–I). These results indicate that CM@YM treatment can restore the microbiota composition at the genus level, as opposed to the DSS group which displayed an imbalance favoring pathogenic or conditionally pathogenic bacteria. Overall, these findings suggest that the modulation of gut microbiota may play a crucial role in the regulatory effects of CM@YM on colitis.

Short-chain fatty acids (SCFA) are fatty acids with less than 6 carbon atoms and are primarily produced in the colon. They are derived from various sources such as food or the fermentation of carbohydrates, proteins, and amino acids by the intestinal flora. SCFA not only serves as nutrient for the body but also plays important biological roles in the organism [52]. A disrupted microbiome can lead to inflammation, disturbance of host metabolism, and alteration in SCFA production in the gut, which can in turn affect the development of diseases [53]. The modulation of probiotic activity by prebiotics is believed to promote the production of SCFA in the colon, which has been shown to inhibit the development of IBD through various mechanisms [54–56]. To evaluate the effect of CM@YM on SCFA production, the content of SCFA was measured using gas chromatography-mass spectrometry (GC-MS). The differences in the content of seven SCFA between the three groups are presented in Fig. 8J as a heat map. The feces of CM@YM-treated mice showed increased levels of acetic acid, propionic acid, and butyric acid compared to the DSS group (Fig. 8K-M). Notably, butyric acid has been extensively studied and demonstrated to play important roles in the regulation of intestinal immune and inflammatory responses. It acts as a natural histone deacetylase (HDAC) inhibitor and serves as a natural ligand for various receptors [57,58].

3.10. Therapeutic effects of CM@YM against DSS-induced colitis

To further establish the superiority of CM@YM, we created a therapeutic model by administering 2.5% DSS in drinking water for one week, followed by oral treatment with various preparations for 5 days to evaluate the therapeutic effect of CM@YM on DSS-induced colitis and to compare it with the clinically used drug 5-aminosalicylic acid (5-ASA) (Fig. 9A). After the cessation of DSS administration, mice with colitis

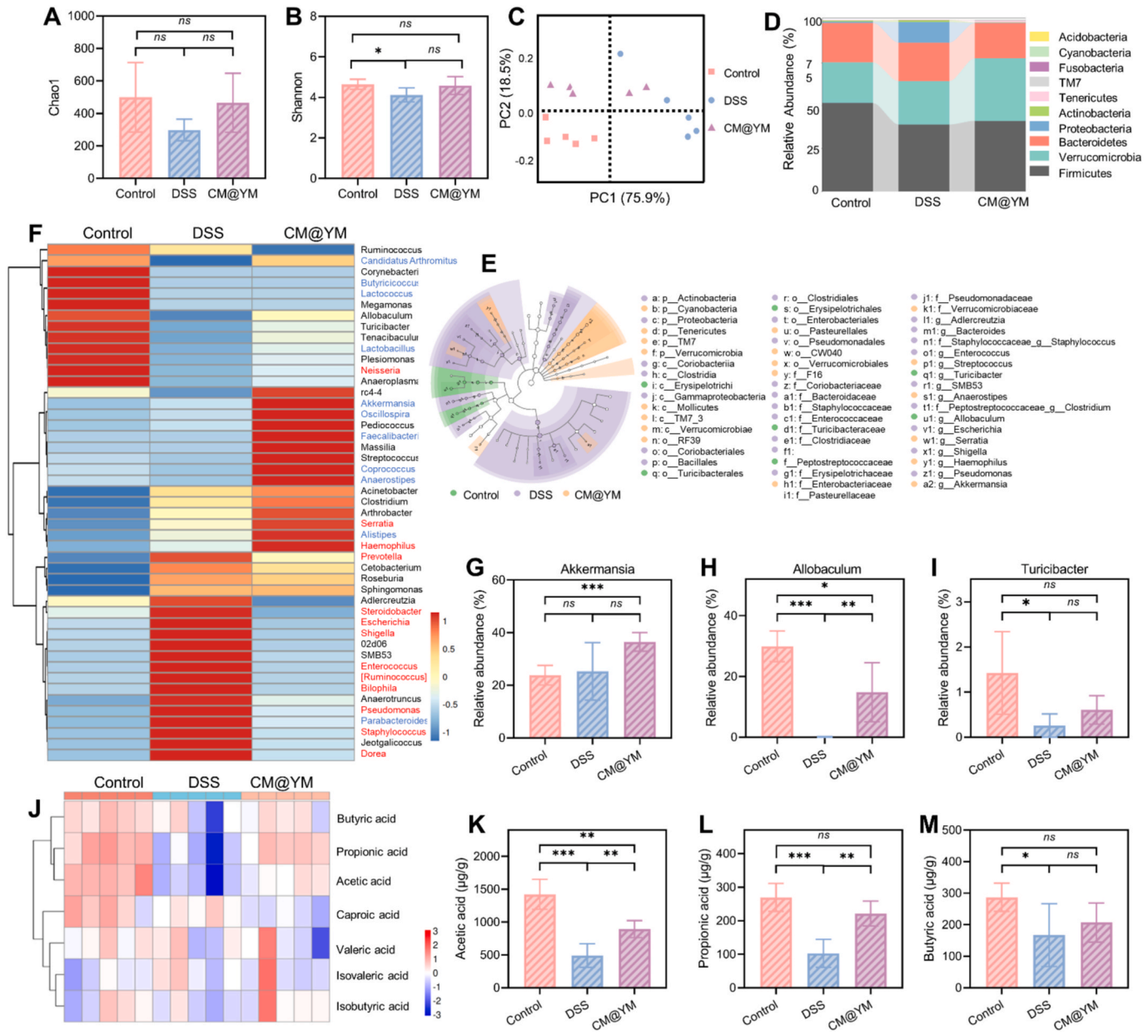

Fig. 8. 16S ribosomal RNA (rRNA) sequencing analysis of gut microbiota regulated by CM@YM. Chao1 (A) and Shannon (B) index of observed OUT displays the ***α***-diversity of the microbial community. (C) PCoA shows the β-diversity of the gut microbiome, each point represents one mouse. (D) Taxonomic bacterial distribution histogram at the phylum level. (E) Cladogram based on LEfSe analysis showing the community composition of the gut microbiota in mice with different treatments. (F) The heatmap shows the relative abundances of microbial compositional profiles at the genus level. (G–I) Significant relative abundance changes at genus levels. (J) Heat map of SCFA levels in mouse feces after different treatments. (K–M) Representative SCFA content in different groups. Data are presented as means ± SD (n = 5; *P < 0.05, **P < 0.01, ***P < 0.001).

were orally treated with saline, 5-ASA, Curcumin, Cur-MPN, and CM@YM for 5 consecutive days. Mice that were not treated with DSS served as the normal group. At 7 days after DSS administration, all mice exhibited weight loss, an increased Disease Activity Index (DAI), and bloody diarrhea, indicating a successful establishment of the DSS-induced colitis model. However, after 5 days of treatment with Curcumin, 5-ASA, Cur-MPN, and CM@YM, the mice in the 5-ASA and CM@YM groups showed the most significant recovery (Fig. 9B and C). The therapeutic effect of CM@YM was also illustrated by changes in spleen and colon length in mice (Fig. 9D–F). Endoscopy results in the CM@YM group also showed healing of ulcerative lesions, which was comparable to that seen in the 5-ASA group (Fig. 9G). H&E staining and endoscopic examination further highlighted the differences between the groups. As depicted in Fig. 9H, the CM@YM group not only restored the disordered arrangement of epithelial cells but also reduced inflammatory cell aggregation and infiltration, leading to tissue restoration to a normal state compared to the model group.

To further validate the efficacy of the CM@YM microcapsules, we measured the expression levels of MPO and pro-inflammatory cytokines (TNF-α, IL-6, IL-1β) in colon homogenates (Fig. 9I-L). The expressions of TNF-α, IL-6, and IL-1β were all significantly reduced after the administration of CM@YM. Furthermore, the application of CM@YM significantly decreased the content of MPO in the colon, bringing it closer to the levels found in normal tissues. These results provide strong evidence for the effectiveness of CM@YM in the delayed treatment of colitis in mice.

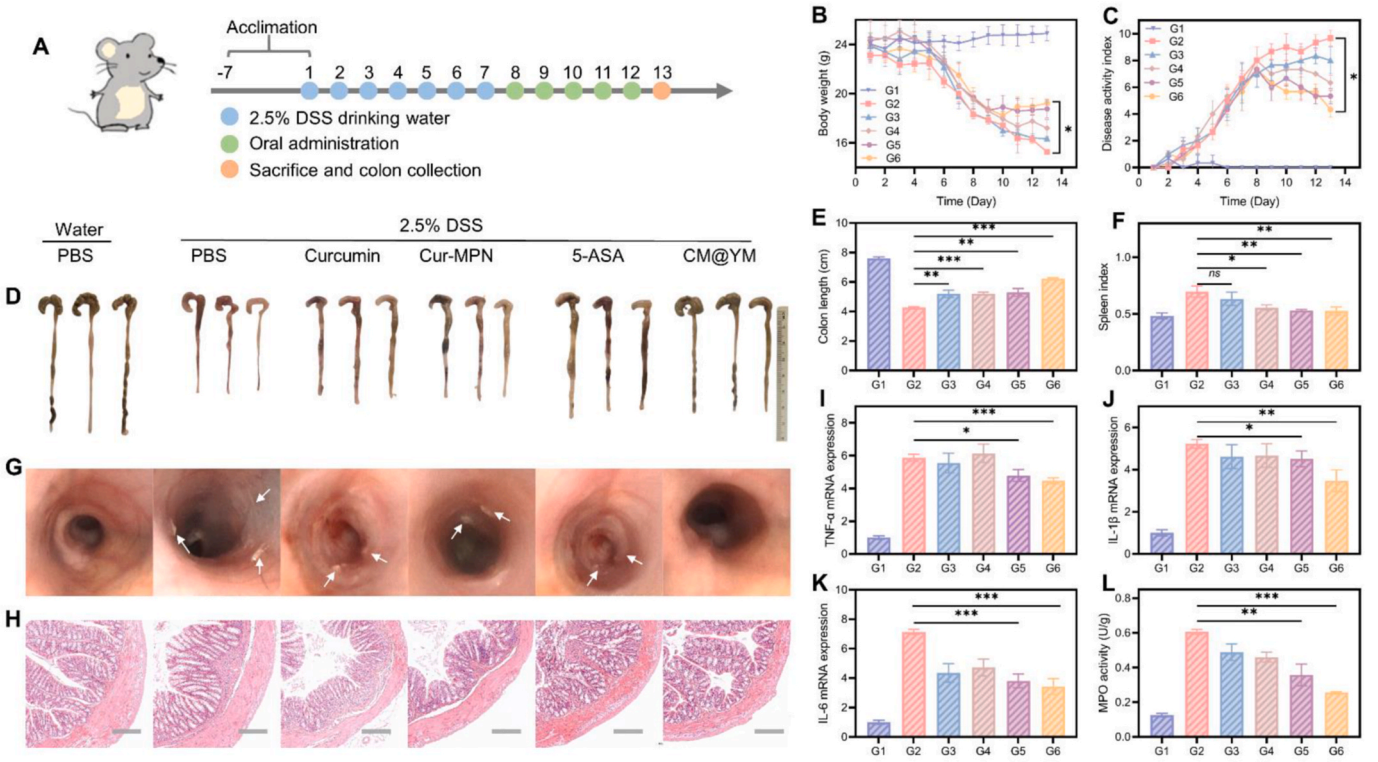

Fig. 9. Therapeutic efficacy of CM@YM against DSS-induced colitis. (A) Schematic showing the experimental procedure for the treatment of DSS-induced colitis mice. (B) Daily body weight over 13 days. (C) DAI score of colitis model mice during the experiment. (D) Photographs of the excised colons from the colitis models on day 13 after treatment. (E) Measurements of colon lengths after different treatments. (F) Measurements of Spleen index after different treatments. (G) Representative photos of the intestinal endoscope of mice treated with the indicated materials on day 13. (H) H&E staining of colonic pathological sections of mice treated with the indicated materials on day 13 (scale bar, 200 μm). The levels of mRNA expression of TNF-α (I), IL-1β (J), and IL-6 (K) in colon tissues. (L) MPO activity in colon tissues was evaluated by the colorimetric method. G1: control group, G2: DSS group, G3: DSS + Cur group, G4: DSS + Cur-MPN group, G5: DSS + 5-ASA group, G6: DSS + CM@YM group. Data are presented as means ± SD (n = 5; *P < 0.05, **P < 0.01, ***P < 0.001).

4. Conclusion

In summary, our study demonstrated that the oral microcapsule CM@YM can effectively treat ulcerative colitis through its anti-oxidant, anti-inflammatory, and intestinal microecological remodeling properties. CM@YM specifically targets the inflamed colon, delivering anti-inflammatory drugs and promoting microecological balance. The CM@YM microcapsule exhibits excellent ROS scavenging ability, stability in the intestinal environment, and biocompatibility with cells and mice. Moreover, CM@YM efficiently targets inflammatory colonic macrophages. In a mouse model of ulcerative colitis, CM@YM treatment effectively alleviated symptoms such as weight loss, colon shortening, and ulceration, while reducing inflammatory cytokines. Furthermore, CM@YM was capable of remodeling the intestinal microbiota and increasing SCFA levels by suppressing harmful bacteria and increasing beneficial bacteria. Although CM@YM demonstrated promising therapeutic effects in the treatment of ulcerative colitis in mice, further investigations are needed to elucidate its mechanisms of action in detail. Additionally, the efficacy of CM@YM in treating chronic enteritis should be explored. In our future work, we will strive to enhance the therapeutic effects of anti-inflammatory systems to treat a wider range of symptoms.

Ethics approval and consent to participate

All animal experiments were performed following the Principles of Laboratory Animal Care and Guidelines of the Laboratory Animal Care Committee of Xi'an Jiaotong University (No: 2021-213).

CRediT authorship contribution statement

Jintao Li: Writing – original draft, Validation, Software, Methodology, Investigation, Formal analysis, Data curation. **Jian Song:** Writing – review & editing, Methodology, Funding acquisition, Formal analysis, Conceptualization. **Zhichao Deng:** Writing – review & editing, Methodology, Funding acquisition, Formal analysis, Conceptualization. **Jian Yang:** Investigation, Data curation. **Xiaoqin Wang:** Investigation, Formal analysis. **Bowen Gao:** Writing – review & editing, Investigation. **Yuanyuan Zhu:** Data curation. **Mei Yang:** Data curation. **Dingpei Long:** Data curation. **Xiaoqin Luo:** Data curation. **Mingxin Zhang:** Writing – review & editing, Supervision, Funding acquisition. **Mingzhen Zhang:** Writing – review & editing, Writing – original draft, Project administration, Funding acquisition, Conceptualization. **Runqing Li:** Supervision, Resources, Project administration, Conceptualization.

Declaration of competing interest

The authors declare that they have no known competing financial interests or personal relationships that could have appeared to influence the work reported in this paper.

Acknowledgments

This work was supported by the National Natural Science Foundation of China (Nos. 52103183, 32360176), the Shaanxi Province Key Research and Development Program (No. 2023-YBSF-072), the Natural Science Basic Research Program of Shaanxi (Nos. 2021JQ-382, 2024JC-YBMS-664), the Fundamental Research Funds for the Central

Universities, China (No. xtr052023008), the Innovation Team of Xi'an Medical University (No. 2021TD15) and the Young Talent Support Plan of Xi'an Jiaotong University, China (No. YX6J001). We thank Dr. Zijun Ren at the Instrument Analysis Center of Xi'an Jiaotong University for assisting with TEM analysis and Dr. Xiaofei Wang at the experimental biomedical center of Xi'an Jiaotong University for his kind assistance with the instrument operation and data analysis.

Appendix A. Supplementary data

Supplementary data to this article can be found online at https://doi.org/10.1016/j.bioactmat.2024.02.033.

References

[1] S.C. Ng, H.Y. Shi, N. Hamidi, Worldwide incidence and prevalence of inflammatory bowel disease in the 21st century: a systematic review of population-based studies, Lancet 390 (10114) (2017) 2768–2778. https://doi.org/10.1016/S0140-6736(17)32448-0.

[2] S.J. Benson-Pope, R.B. Gearry, Editorial: increasing IBD prevalence and its complications in the context of the COVID-19 pandemic, Aliment. Pharmacol. Ther. 51 (12) (2020) 1441–1442. https://doi.org/10.1111/apt.15769.

[3] M. De Gregorio, B. D'Souza, W. Connell, M.A. Kamm, R. Woods, S.J. Connor, A. J. Thompson, N.S. Ding, Suboptimal disease control is common in patients with Crohn's perianal fistulas with capacity to optimise medical and surgical treatment in real-world experience: a cross-sectional analysis of baseline disease characteristics in the FINESS study, J Crohns Colitis 17 (2023) 666. https://doi.org/10.1093/ecco-jcc/jjac190.0668.

[4] T. Tian, Z.L. Wang, J.H. Zhang, Pathomechanisms of oxidative stress in inflammatory bowel disease and potential antioxidant therapies, Oxid. Med. Cell. Longev. 2017 (2017), 4535194, https://doi.org/10.1155/2017/4535194.

[5] A. Larabi, N. Barnich, H.T.T. Nguyen, New insights into the interplay between autophagy, gut microbiota and inflammatory responses in IBD, Autophagy 16 (1) (2020) 38–51. https://doi.org/10.1080/15548627.2019.1635384.

[6] A. Lavelle, H. Sokol, Gut microbiota-derived metabolites as key actors in inflammatory bowel disease, Nat. Rev. Gastroenterol. Hepatol. 17 (4) (2020) 223–237. https://doi.org/10.1038/s41575-019-0258-z.

[7] Z.Z. Zhang, Y. Pan, Z.Y. Guo, X. Fan, Q.Q. Pan, W.X. Gao, K. Luo, Y.J. Pu, B. He, An olsalazine nanoneedle-embedded inulin hydrogel reshapes intestinal homeostasis in inflammatory bowel disease, Bioact. Mater. 33 (2024) 71–84. https://doi.org/10.1016/j.bioactmat.2023.10.028.

[8] X. Fan, Z.Z. Zhang, W.X. Gao, Q.Q. Pan, K. Luo, B. He, Y.J. Pu, An engineered butyrate-derived polymer nanoplatform as a mucosa-healing enhancer potentiates the therapeutic effect of Magnolol in inflammatory bowel disease, ACS Nano 18 (1) (2023) 229–244. https://doi.org/10.1021/acsnano.3c05732.

[9] C.C. Bain, C.L. Scott, A.M. Mowat, Resident and pro-inflammatory macrophages in the colon represent alternative context dependent fates of the same Ly6Chi monocyte precursors, Immunology 137 (2012) 218. https://doi.org/10.1038/mi.2012.89.

[10] J.W.O. Ballard, S.G. Towarnicki, Mitochondria, the gut microbiome and ROS, Cell. Signal. 75 (2020), 109737, https://doi.org/10.1016/j.cellsig.2020.109737.

[11] K.M. Au, J.E. Wilson, J.P.Y. Ting, A.Z. Wang, An injectable subcutaneous colon-specific immune niche for the treatment of ulcerative colitis, Nat. Biomed. Eng. (2023). https://doi.org/10.1038/s41551-023-01136-9.

[12] C. Lautenschläger, C. Schmidt, D. Fischer, A. Stallmach, Drug delivery strategies in the therapy of inflammatory bowel disease, Adv. Drug Deliv. Rev. 71 (2014) 58–76. https://doi.org/10.1016/j.addr.2013.10.001.

[13] C.N. Bernstein, M. Fried, J.H. Krabshuis, H. Cohen, R. Eliakim, S. Fedail, R. Gearry, K.L. Goh, S. Hamid, A.G. Khan, A.W. LeMair, Malfertheiner, O.Y. Qin, J.F. Rey, A. Sood, F. Steinwurz, O.O. Thomsen, A. Thomson, G. Watermeyer, World gastroenterology organization practice Guidelines for the diagnosis and management of IBD in 2010, Inflamm. Bowel Dis. 16 (1) (2010) 112–124. https://doi.org/10.1002/ibd.21048.

[14] Z.B. Cai, S. Wang, J.N. Li, Treatment of inflammatory bowel disease: a comprehensive review, Front. Med. 8 (2021), 765474, https://doi.org/10.3389/fmed.2021.765474.

[15] A. Stallmach, S. Hagel, T. Bruns, Adverse effects of biologics used for treating IBD, Best Pract. Res. Clin. Gastroenterol. 24 (2) (2010) 167–182. https://doi.org/10.1016/j.bpg.2010.01.002.

[16] M. Argollo, P.G. Kotze, P. Kakkadasam, G. D'Haens, Optimizing biologic therapy in IBD: how essential is therapeutic drug monitoring? Nat. Rev. Gastroenterol. Hepatol. 17 (11) (2020) 702–710. https://doi.org/10.1038/s41575-020-0352-2.

[17] J. Wise, Glucocorticoids may increase risk of serious blood infection, Br. Med. J. 353 (2016) i3230, https://doi.org/10.1136/bmj.i3230.

[18] F. Berrnejo, M. Aguas, M. Chaparro, E. Domènech, A. Echarri, E. García-Planella, I. Guerra, J.P. Gisbert, A. López-Sanromán, Recommendations of the Spanish working group on Crohn's disease and ulcerative colitis (GETECCU) on the use of tiopurines in inflammatory bowel disease, Gastroenterol. Hepatol. 41 (3) (2018) 205–221. https://doi.org/10.1016/j.gastrohep.2017.11.007.

[19] M. Duran-Lobato, Z.G. Niu, M.J. Alonso, Oral delivery of biologics for precision medicine, Adv. Mater. 32 (13) (2020), 1901935, https://doi.org/10.1002/adma.201901935.

[20] X.L. Pu, N.J. Ye, M.S. Lin, Q.Y. Chen, L.L. Dong, H.T. Xu, R.F. Luo, X.Q. Han, S. S. Qi, W.B. Nie, H.Q. He, Y.L. Wang, L.X. Dai, D.S. Lin, F. Gao, β-1,3-D-Glucan based yeast cell wall system loaded emodin with dual-targeting layers for ulcerative colitis treatment, Carbohydr. Polym. 273 (2021), 111682, https://doi.org/10.1016/j.carbpol.2021.118612.

[21] Q.Y. Chen, R.F. Luo, X.Q. Han, J.M. Zhang, Y. He, S.S. Qi, X.L. Pu, W.B.A. Nie, L. L. Dong, H.T. Xu, F. Liu, M.S. Lin, H.Y. Zhong, C.M. Fu, F. Gao, Entrapment of macrophage-target nanoparticles by yeast microparticles for Rhein delivery in ulcerative colitis treatment, Biomacromolecules 22 (6) (2021) 2754–2767. https://doi.org/10.1021/acs.biomac.1c00425.

[22] P.R. Taylor, S.V. Tsoni, J.A. Willment, K.M. Dennehy, M. Rosas, H. Findon, K. Haynes, C. Steele, M. Botto, S. Gordon, G.D. Brown, Dectin-1 is required for β-glucan recognition and control of fungal infection, Nat. Immunol. 8 (1) (2007) 31–38. https://doi.org/10.1038/ni1408.

[23] G.C.F. Chan, W.K. Chan, D.M.Y. Sze, The effects of β-glucan on human immune and cancer cells, J. Hematol. Oncol. 2 (2009), 25, https://doi.org/10.1186/1756-8722-2-25.

[24] X.J. Zhang, X.Q. Xu, Y.D. Chen, Y. Dou, X. Zhou, L.L. Li, C.W. Li, H.J. An, H. Tao, H. Y. Hu, X.H. Li, J.X. Zhang, Bioinspired yeast microcapsules loaded with self-assembled nanotherapies for targeted treatment of cardiovascular disease, Mater. Today 20 (6) (2017) 301–313. https://doi.org/10.1016/j.mattod.2017.05.006.

[25] D. Panwar, A. Shubhashini, M. Kapoor, Complex alpha and beta mannan foraging by the human gut bacteria, Biotechnol. Adv. 66 (2023), 108166, https://doi.org/10.1016/j.biotechadv.2023.108166.

[26] U.P. Tiwari, S.A. Fleming, M.S.A. Rasheed, R. Jha, R.N. Dilger, The role of oligosaccharides and polysaccharides of xylan and mannan in gut health of monogastric animals, J. Nutr. Sci. 9 (2020) e21, https://doi.org/10.1017/jns.2020.14.

[27] J.L. Yang, G.Z. Zhang, M.Y. Peng, S.C. Tan, S.C. Ge, X.Y. Yang, Y. Liang, Z.Y. Wen, L. Xie, T.H. Zhou, S.X. Wu, J.Y. An, Y.F. Wang, W. Liu, K.X. Zhang, Z.Z. Zhang, J. J. Liu, J.J. Shi, Bionic regulators break the ecological niche of pathogenic bacteria for modulating dysregulated microbiome in colitis, Adv. Mater. 34 (39) (2022), 2204650, https://doi.org/10.1002/adma.202204650.

[28] A. Giordano, G. Tommonaro, Curcumin and cancer, Nutrients 11 (10) (2019), 2376, https://doi.org/10.3390/nu11102376.

[29] M. Pulido-Moran, J. Moreno-Fernandez, C. Ramirez-Tortosa, M.C. Ramirez-Tortosa, Curcumin and health, Molecules 21 (3) (2016), 264, https://doi.org/10.3390/molecules21030264.

[30] S. Hasanzadeh, M.I. Read, A.R. Bland, M. Majeed, T. Jamialahmadi, A. Sahebkar, Curcumin: an inflammasome silencer, Pharmacol. Res. 159 (2020), 104921m, https://doi.org/10.1016/j.phrs.2020.104921.

[31] V. Zoi, V. Galani, G.D. Lianos, S. Voulgaris, A.P. Kyritsis, G.A. Alexiou, The role of curcumin in cancer treatment, Biomedicines 9 (9) (2021), 1086, https://doi.org/10.3390/biomedicines9091086.

[32] P. Anand, A.B. Kunnumakkara, R.A. Newman, B.B. Aggarwal, Bioavailability of curcumin: problems and promises, Mol. Pharm. 4 (6) (2007) 807–818. https://doi.org/10.1021/mp700113r.

[33] G. Appendino, P. Allegrini, E. de Combarieu, F. Novicelli, G. Ramaschi, N. Sardone, Shedding light on curcumin stability, Fitoterapia 156 (2022), 105084, https://doi.org/10.1016/j.fitote.2021.105084.

[34] J.L. Guo, Y. Ping, H. Ejima, K. Alt, M. Meissner, J.J. Richardson, Y. Yan, K. Peter, D. von Elverfeldt, C.E. Hagemeyer, F. Caruso, Engineering multifunctional capsules through the assembly of metal-phenolic networks, Angew. Chem., Int. Ed. 53 (22) (2014) 5546–5551. https://doi.org/10.1002/anie.201311136.

[35] X.Y. Liang, M. Mu, B. Chen, D. Chuan, N. Zhao, R.R. Fan, X. Tang, H.F. Chen, B. Han, G. Guo, BSA-assisted synthesis of nanoreactors with dual pH and glutathione responses for ferroptosis and photodynamic synergistic therapy of colorectal cancer, Mater Today Adv 16 (2022), 100308, https://doi.org/10.1016/j.mtadv.2022.100308.

[36] S. Lee, Y.Y. Chang, J. Lee, S.K.M. Perikamana, E.M. Kim, Y.H. Jung, J.H. Yun, H. Shin, Surface engineering of titanium alloy using metal-polyphenol network coating with magnesium ions for improved osseointegration, Biomater. Sci. 8 (12) (2020) 3404–3417. https://doi.org/10.1039/D0BM00566E.

[37] Y.Y. Chen, D. Jia, Q.M. Wang, Y.R. Sun, Z.A. Rao, X.J. Lei, J.C. Zhao, K.F. Zeng, Z. G. Xu, J. Ming, Promotion of the anticancer activity of curcumin based on a metal-polyphenol networks delivery system, Int. J. Pharm. 602 (2021), 120650, https://doi.org/10.1016/j.ijpharm.2021.120650.

[38] Y.Z. Zhang, Y.Y. Li, Inflammatory bowel disease: pathogenesis, world, J. Gastroenterol. 20 (1) (2014) 91–99. https://doi.org/10.3748/wjg.v20.i1.91.

[39] D. Dai, J.Y. Zhu, C.Q. Sun, M. Li, J.X. Liu, S.C. Wu, K. Ning, L.J. He, X.M. Zhao, W. H. Chen, GMrepo v2: a curated human gut microbiome database with special focus on disease markers and cross-dataset comparison, Nucleic Acids Res. 50 (D1) (2022) D777–D784. https://doi.org/10.1093/nar/gkab1019.

[40] H.Z. Tan, J.X. Zhao, H. Zhang, Q.X. Zhai, W. Chen, Novel strains of Bacteroides fragilis and Bacteroides ovatus alleviate the LPS-induced inflammation in mice, Appl. Microbiol. Biotechnol. 103 (5) (2019) 2353–2365. https://doi.org/10.1007/s00253-019-09617-1.

[41] A. Mukherjee, C. Lordan, R.P. Ross, P.D. Cotter, Gut microbes from the phylogenetically diverse genusand their various contributions to gut health, Gut Microb. 12 (1) (2020), 1802866, https://doi.org/10.1080/19490976.2020.1802866.

[42] X.L. Wang, X.L. Li, X.Y. Liang, J.Y. Liang, C. Zhang, J. Yang, C. Wang, D.L. Kong, H. F. Sun, ROS-responsive capsules engineered from green tea polyphenol-metal networks for anticancer drug delivery, J. Mater. Chem. B 6 (7) (2018) 1000–1010. https://doi.org/10.1039/C7TB02688A.

[43] J.W. Duan, Z.G. Chen, X.Y. Liang, Y.L. Chen, H.Y. Li, X.X. Tian, M.M. Zhang, X. L. Wang, H.F. Sun, D.L. Kong, Y.J. Li, J. Yang, Construction and application of therapeutic metal-polyphenol capsule for peripheral artery disease, Biomaterials 255 (2020), 120199, https://doi.org/10.1016/j.biomaterials.2020.120199.

[44] J.L. Xu, Q.L. Ma, Y. Zhang, Z.Y. Fei, Y.F. Sun, Q. Fan, B. Liu, J.Y. Bai, Y. Yu, J. H. Chu, J.R. Chen, C. Wang, Yeast-derived nanoparticles remodel the immunosuppressive microenvironment in tumor and tumor-draining lymph nodes to suppress tumor growth, Nat. Commun. 13 (1) (2022), 110, https://doi.org/10.1038/s41467-021-27750-2.

[45] J. Liu, L.K. Zhang, W.J. Hu, R. Tian, Y.Z. Teng, C.Y. Wang, Preparation of konjac glucomannan-based pulsatile capsule for colonic drug delivery system and its evaluation in vitro and in vivo, Carbohydr. Polym. 87 (1) (2012) 377–382. https://doi.org/10.1016/j.carbpol.2011.07.062.

[46] J.Q. Xu, T.J. Chu, T.T. Yu, N.S. Li, C.L. Wang, C. Li, Y.L. Zhang, H. Meng, G.J. Nie, Design of diselenide-bridged hyaluronic acid nano-antioxidant for efficient ROS scavenging to relieve colitis, ACS Nano 16 (8) (2022) 13037–13048. https://doi.org/10.1021/acsnano.2c05558.

[47] Y.Y. Zeng, M.N. Fan, Q. Zhou, D.F. Chen, T. Jin, Z.X. Mu, L. Li, J.L. Chen, D.C. Qiu, Y.M. Zhang, Y.H. Pan, X.K. Shen, X.J. Cai, Reactive oxygen species-activated CO versatile nanomedicine with innate gut immune and microbiome remodeling effects for treating inflammatory bowel disease, Adv. Funct. Mater. 33 (2023), 2304381, https://doi.org/10.1002/adfm.202304381.

[48] Y. Ma, S.Q. Gou, Z.H. Zhu, J.F. Sun, M.A. Shahbazi, T.Y. Si, C. Xu, J.L. Ru, X.X. Shi, R.L. Reis, S.C. Kundu, B.W. Ke, G.J. Nie, B. Xiao, Transient mild photothermia improves therapeutic performance of oral nanomedicines with enhanced accumulation in the colitis mucosa, Adv. Mater. (2024), 2309516, https://doi.org/10.1002/adma.202309516.

[49] Y.R. Na, M. Stakenborg, S.H. Seok, G. Matteoli, Macrophages in intestinal inflammation and resolution: a potential therapeutic target in IBD, Nat. Rev. Gastroenterol. Hepatol. 16 (9) (2019) 531–543. https://doi.org/10.1038/s41575-019-0172-4.

[50] P.J. Koelink, F.M. Bloemendaal, B.F. Li, L. Westera, E.W.M. Vogels, M. van Roest, A.K. Gloudemans, A.B. van't Wout, H. Korf, S. Vermeire, A.A. te Velde, C. Y. Ponsioen, G.R.A.M. D'Haens, J.S. Verbeek, T.L. Geiger, M.E. Wildenberg, G. R. van den Brink, Anti-TNF therapy in IBD exerts its therapeutic effect through macrophage IL-10 signalling, Gut 69 (6) (2020) 1053–1063. https://doi.org/10.1136/gutjnl-2019-318264.

[51] P.J. Murray, Macrophage polarization, Annu. Rev. Physiol. 79 (2017) 541–566. https://doi.org/10.1146/annurev-physiol-022516-034339.

[52] C. Martin-Gallausiaux, L. Marinelli, H.M. Blottière, P. Larraufie, N. Lapaque, SCFA: mechanisms and functional importance in the gut, Proc. Nutr. Soc. 80 (1) (2021) 37–49. https://doi.org/10.1017/S0029665120006916.

[53] J.K. Tan, L. Macia, C.R. Mackay, Dietary fiber and SCFAs in the regulation of mucosal immunity, J. Allergy Clin. Immunol. 151 (2) (2023) 361–370. https://doi.org/10.1016/j.jaci.2022.11.007.

[54] F. Bishehsari, P. Engen, N.Z. Preite, Y.E. Tunçil, A. Naqib, M. Shaikh, M. Rossi, S. Wilber, S. Green, B.R. Hamaker, K. Khazaie, R.M. Voigt, C.B. Forsyth, A. Keshavarzian, Prebiotic treatment corrects composition of gut microbiota, promotes scfa production, and suppresses colon carcinogenesis, Gastroenterology 154 (6) (2018). S200, https://doi.org/10.1016/S0016-5085(18)31070-9.

[55] R.F. McLoughlin, B.S. Berthon, M.E. Jensen, K.J. Baines, L.G. Wood, Short-chain fatty acids, prebiotics, synbiotics, and systemic inflammation: a systematic review and meta-analysis, Am. J. Clin. Nutr. 106 (3) (2017) 930–945. https://doi.org/10.3945/ajcn.117.156265.

[56] Z.L. Zhang, H. Zhang, T. Chen, L. Shi, D.R. Wang, D. Tang, Regulatory role of short-chain fatty acids in inflammatory bowel disease, Cell Commun. Signal. 20 (1) (2022), 64, https://doi.org/10.1186/s12964-022-00869-5.

[57] X.H. Zhu, K. Li, G.C. Liu, R. Wu, Y. Zhang, S.Y. Wang, M. Xu, L.G. Lu, P. Li, Microbial metabolite butyrate promotes anti-PD-1 antitumor efficacy by modulating T cell receptor signaling of cytotoxic CD8 T cell, Gut Microb. 15 (2) (2023), 2249143, https://doi.org/10.1080/19490976.2023.2249143.

[58] M.B. Zhang, Y.A. Wang, X.Q. Zhao, C. Liu, B.Z. Wang, J. Zhou, Mechanistic basis and preliminary practice of butyric acid and butyrate sodium to mitigate gut inflammatory diseases: a comprehensive review, Nutr. Res. 95 (2021) 1–18. https://doi.org/10.1016/j.nutres.2021.08.007.